nature neuroscience

Glia initiate brain assembly through noncanonical Chimaerin–Furin axon guidance in *C. elegans*

Georgia Rapti[1], Chang Li[1,2], Alan Shan[1,2], Yun Lu[1] & Shai Shaham[1]

Brain assembly is hypothesized to begin when pioneer axons extend over non-neuronal cells, forming tracts guiding follower axons. Yet pioneer-neuron identities, their guidance substrates, and their interactions are not well understood. Here, using time-lapse embryonic imaging, genetics, protein-interaction, and functional studies, we uncover the early events of *C. elegans* brain assembly. We demonstrate that *C. elegans* glia are key for assembly initiation, guiding pioneer and follower axons using distinct signals. Pioneer sublateral neurons, with unique growth properties, anatomy, and innervation, cooperate with glia to mediate follower-axon guidance. We further identify a Chimaerin (CHIN-1)– Furin (KPC-1) double-mutant that severely disrupts assembly. CHIN-1 and KPC-1 function noncanonically, in glia and pioneer neurons, for guidance-cue trafficking. We exploit this bottleneck to define roles for glial Netrin and Semaphorin in pioneer- and follower-axon guidance, respectively, and for glial and pioneer-neuron Flamingo (CELSR) in follower-axon navigation. Taken together, our studies reveal previously undescribed glial roles in pioneer-axon guidance, suggesting conserved principles of brain assembly.

Brain formation requires an astonishing orchestration of events, including process fasciculation, axon–substrate interactions, and target-cell recognition. Assembly is thought to initiate when the first axons extend along non-neuronal cells[1]. Since these events occur in the embryo, where live imaging and functional studies are difficult, identifying pioneer axons and their guidance substrates has been challenging.

Glia physically associate with major axon tracts and also express guidance cues[2]. Some studies in grasshopper embryos and Drosophila larvae suggest glial roles in axon guidance, while other invertebrate studies instead propose glial roles in axon fasciculation[3–7]. Moreover, whether glia direct pioneer-axon guidance in these systems is not resolved. Similarly, glial contributions to axon guidance in the mammalian central nervous system, and specifically to the guidance of pioneer axons, remain unclear[8,9]. The requirement of glia for neuronal viability adds additional experimental complexity.

Guidance and cell-adhesion proteins that control axon navigation have been described[10]. Functional studies of these factors suggest that they account for only select guidance decisions within the hundred-billion-neuron mammalian brain. Thus, unknown components may be necessary to fully explain brain self-assembly. Genetic redundancies may also account for the highly specific axon-guidance defects seen in animals disrupted for broadly expressed genes[11] and may explain why eliminating multiple genes is necessary to elicit guidance defects[12].

With unbiased gene-function discovery approaches[13], invariant embryonic development[14], and glial cells dispensable for neuronal viability[15], the nematode *Caenorhabditis elegans* is a powerful arena in which to decipher cellular and molecular events governing brain assembly. The *C. elegans* brain neuropil, the nerve ring (NR), consists of >170 sensory, motor, and interneuron processes tightly bundled around the pharynx[16] and is enveloped by processes of four CEPsh glia. Axons entering the NR are arranged in bundles (for example, bilateral amphid, deirid, and sublateral commissures containing 23, 5, and 12 axons, respectively) or occupy noncommissural paths (for example, the AIY interneuron; see below). Little is known about NR assembly. Some *C. elegans* mutants in genes affecting peripheral nerve guidance exhibit partially penetrant NR navigation defects for some neurons[17–19]. Other genes, including *cwn-2* (which encodes the *C. elegans* homolog of Wnt5), functioning in sublateral commissure (SubL) neurons, control overall NR placement[20]. Nonetheless, identities of NR pioneer cells and their functions, as well as factors affecting overall NR integrity, are not known and have been the subject of extensive speculation[21,22].

Here we demonstrate that *C. elegans* CEPsh glia promote key early events in NR assembly by directing the extension of a pioneer-axon fascicle composed of SubL neurons. Glia and pioneer neurons extend coalescing processes to generate the NR, and they cooperatively direct follower-axon NR entry. We identify a mutant, defective in both CHIN-1 (Chimaerin) and KPC-1 (Furin), in which NR entry is blocked for >70% of axons. These proteins cooperate in glia and pioneer neurons to regulate guidance-cue trafficking and define a choke point we use to identify a network of redundant guidance factors, some specifically required in glia, for NR assembly. Our studies identify pioneer neurons with unique properties and evoke comparisons between CEPsh glia and vertebrate radial glia, defining the initial steps of assembly of an animal brain at single-cell resolution.

RESULTS

CEPsh glia and SubL neurons pioneer the NR and guide its assembly

The *C. elegans* postembryonic NR is comprised of several neuronal commissures and is surrounded by four CEPsh glial cells (**Fig. 1a**,**b**).

[1]Laboratory of Developmental Genetics, The Rockefeller University, New York, New York, USA. [2]These authors contributed equally to this work. Correspondence should be addressed to G.R. (grapti@rockefeller.edu) or S.S. (shaham@rockefeller.edu).

Received 27 April; accepted 19 July; published online 28 August 2017; doi:10.1038/nn.4630

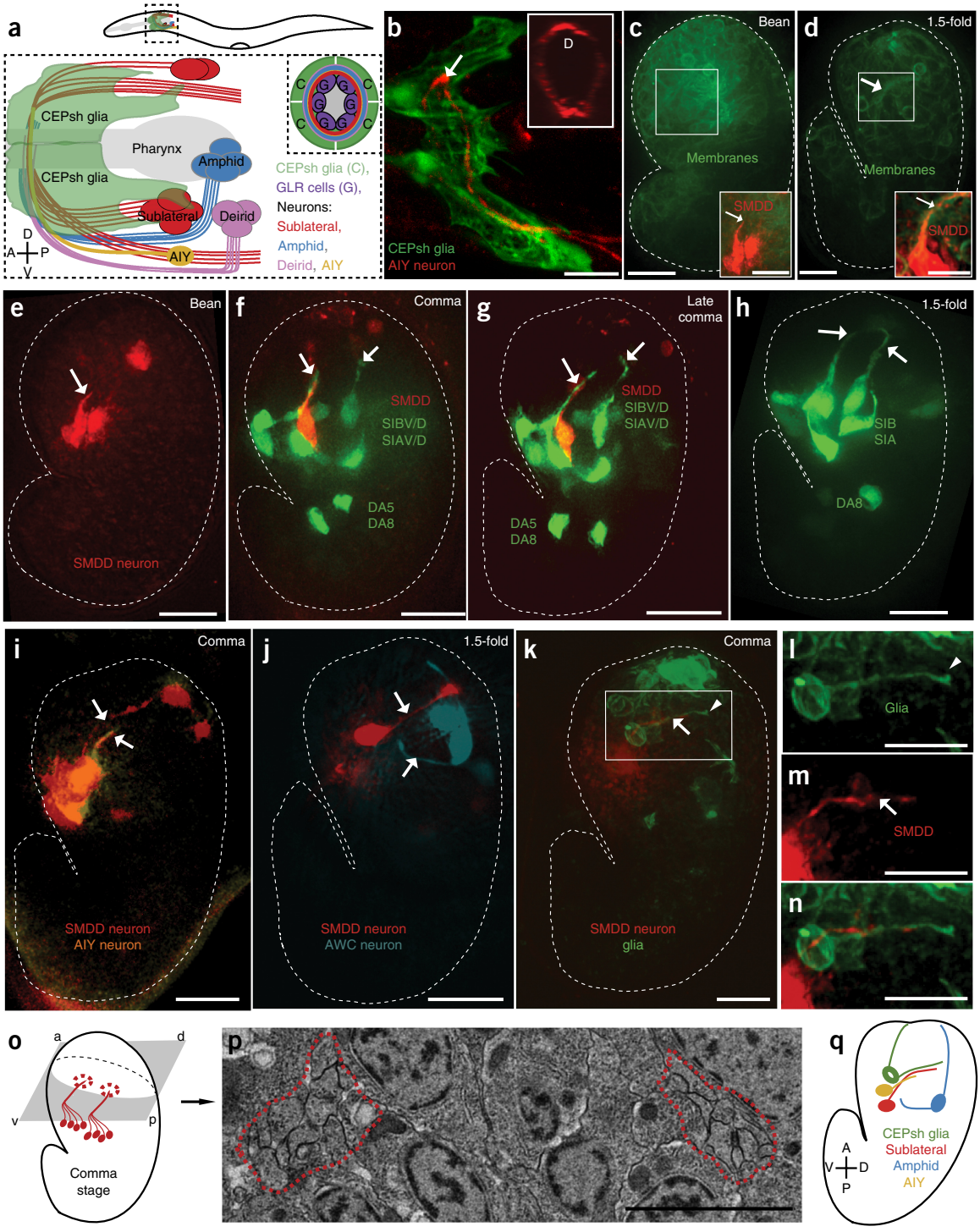

Figure 1 Hierarchical assembly of the embryonic NR. (**a**–**b**) The postembryonic NR is populated by neuronal commissures and enveloped by CEPsh glia. (**a**) Schematic of lateral view of postembryonic NR. (**b**) Imaging of postembryonic NR in L4 animals. Inset: cross-sectional view. AIY, *Pttx-3::mCherry* (red); CEPsh glia, *Phlh-17::myristoylated-GFP*. (**c**–**n**) Formation of the embryonic NR starts at late bean stage, with early entry of SubL axons and CEPsh glia, and later entry of other components. (**c**,**d**) *Phis-72::myristoylated-GFP* (cell membranes). Insets: enlarged view of white rectangle in **c** and **d** with the addition of the reporter used in **e**. (**c**–**k**) Dotted line: embryo outline. D, dorsal; V, ventral; A, anterior; P, posterior. Arrow, axon; arrowhead (in **k** and **l**), CEPsh glia. Scale bars, 10 µm. (**c**–**g**,**i**–**k**,**m**,**n**) *Pttx-3::mCherry* (SMDD, red; AIY, pseudocolored orange in **i**). (**e**–**h**) *Pceh-17::GFP*, SubL neurons SIAV, SIAD, SIBV, land SIBD. (**j**) *Phlh-16::GFP* (SIA and SIB, red; AWC, pseudocolored blue). (**k**–**n**) *Pmir-228::myristoylated-GFP* (glia). (**b**–**n**) Expression patterns are described in Online Methods and **Supplementary Tables 8** and **10**. (**l**–**n**) magnified view of boxed region in **k**. (**o**,**p**) A single pair of bilateral bundles are observed in electron micrographs of early comma stage embryos. Schematic (**o**) and magnification (**p**) of electron micrograph section. The magnified region corresponds to the region outlined in the blue box of **Supplementary Fig. 1g**. Red outline, axon bundle; scale bar, 2 µm. (**q**) Summary of imaging results (also see **Supplementary Fig. 2**). CEPsh glia and pioneer neurons enter the NR path first, followed by amphid and AIY neurons.

A corresponding compact, process-rich structure can be seen around the pharynx of 1.5-fold embryos (440 min postfertilization; **Supplementary Fig. 1d**,**h**), but not in earlier comma-stage embryos (400 min; **Supplementary Fig. 1c**,**g**), as observed by electron microscopy (EM) or fluorescence imaging of a ubiquitously expressed membrane–GFP reporter (**Fig. 1c**,**d**). Thus, NR assembly initiates between these stages. To study NR formation, we therefore imaged axons of the amphid (AWC, AFD, ASE, and AUA), deirid (ADA and BDU), and SubL (SIA, SIB, and SMD) commissures, as well as noncommissural neurons (including AIY and BAG) between 360 and 450 min of development. Five bilateral pairs of SubL axons (SIAV, SIAD, SIBV, SIBD, and SMDD) enter the NR earlier than any other axons we examined. These emerge ventrally and coalesce in left–right bilateral bundles in bean-stage embryos (**Fig. 1e**,**f**), cross the lateral midline (which we define as 'NR entry') at comma stage, and meet to form a ring-like structure by the 1.5-fold embryonic stage (**Fig. 1g**,**h**). Other axons enter the NR later and at different times. Axons of AIY interneurons (**Fig. 1i**) and BAG neurons, for example, emerge at the comma stage, only to enter the NR at the 1.5-fold stage (**Supplementary Fig. 2e**,**f**). NR entry timing can be sequential within nonpioneer commissures: AWC amphid commissure axons extend at late bean stage, entering the NR in 1.5-fold embryos (**Fig. 1j**), while co-commissural AFD and AUA axons emerge at the comma stage, entering the NR only in two-fold embryos (**Supplementary Fig. 2f**–**h**,**i**,**l**). ASE amphid-commissure axons and the deirid commissure axons BDU and ADA enter the NR even later, after the two-fold stage (**Supplementary Fig. 2j**,**m**–**q**).

Notably, processes of ventral CEPsh glia coalesce with SubL axons early (**Fig. 1k**–**n**), defining the presumptive NR. Thus, dorsal extension of a ventrally located process bundle composed, at least in part, of CEPshV glia, SIAV, SIAD, SIBV, SIBD, and SMDD processes is a very early event in NR formation. Supporting this notion, EM of an early comma-stage embryo revealed a single pair of bilateral bundles, each composed of 10 or fewer processes (**Fig. 1o**,**p**). Muscle arms, abutting the inner surface of the postembryonic NR[16], are not aligned with the early NR tract (**Supplementary Fig. 2r**–**u**). Thus, the NR is pioneered by a small, well-defined group of axons and glial processes, with subsequent orderly addition of other axons (**Fig. 1q**).

To determine whether orderly assembly reflects a functional hierarchy, we ablated early NR entrants by expressing the pro-apoptotic BH3-only protein EGL-1 before axon outgrowth and scored cell death by the absence of cell-specific markers in larvae (Online Methods). Ablation of either ventral or dorsal CEPsh glia correlated with AIY axon NR entry defects (**Fig. 2a**–**d** and **Supplementary Table 1**) and with guidance defects of AWB and AWC co-commissural amphid axons (5 of 21 animals; ref. 23). The SubL bundle enters the NR in CEPsh glia-ablated animals; however, it often defasciculates, extending aberrantly anterior to the NR (**Fig. 2e**–**h** and **Supplementary Table 1**). Since SubL neurons enter the NR in CEPsh glia-ablated animals, glial effects on follower-axon guidance are at least partially independent of SubL neurons. Conversely, SIA and SIBV (SubL) neuron ablation correlates with defects in AIY axons (**Fig. 2i**–**l** and **Supplementary Table 1**) and in amphid-commissure axon NR entry (25 of 54 animals) but spares CEPsh glia process growth and NR wrapping (**Fig. 2m**–**p** and **Supplementary Table 1**).

In summary, the NR is hierarchically assembled: CEPsh glia processes and early-fasciculating SubL axons grow together to mark the presumptive NR. The NR is then populated, in an orderly fashion, by noncommissural, amphid-commissure, and deirid-commissure axons. CEPsh glia promote SubL neuron fasciculation, while CEPsh glia and SubL neurons cooperatively guide follower-axon NR entry.

A NR-assembly-defective mutant reveals cooperative guidance roles for KPC-1 (Furin) and CHIN-1 (Chimaerin)

To understand the molecular basis of pioneer-neuron and CEPsh glia functions, we performed a genetic screen, seeking mutants exhibiting AWC- or ASE-axon NR entry defects reminiscent of CEPsh glia-ablated animals (Online Methods). True-breeding mutants were subjected to whole-genome sequencing, genetic mapping, and rescue studies. Besides recovering weakly penetrant mutants in known guidance genes[18], we found one mutant, exhibiting uncoordinated movement and highly penetrant ASE and AWC axon NR entry defects (**Fig. 3a**–**b**,**o**), with no lesion in known *C. elegans* guidance genes.

NR entry defects in this mutant were prominent (>70%) in all follower neurons examined, including another amphid-commissure neuron (AFD) in and the noncommissural interneurons AIY and PVQ (**Fig. 3c**–**h**,**o**). Defective axons often failed to extend dorsally, resulting in NR gaps when viewed in cross section (**Fig. 3e**,**f**). This was accompanied by loss of *str-2* expression in AWC neurons (**Fig. 3o**), which depends on bilateral axon contacts[24]. Focused ion beam scanning electron microscopy reconstructions of newly hatched larvae revealed that ventral aspects of wild-type and mutant NRs contained roughly similar axon numbers, but lateral and dorsal aspects of the mutant NR had markedly

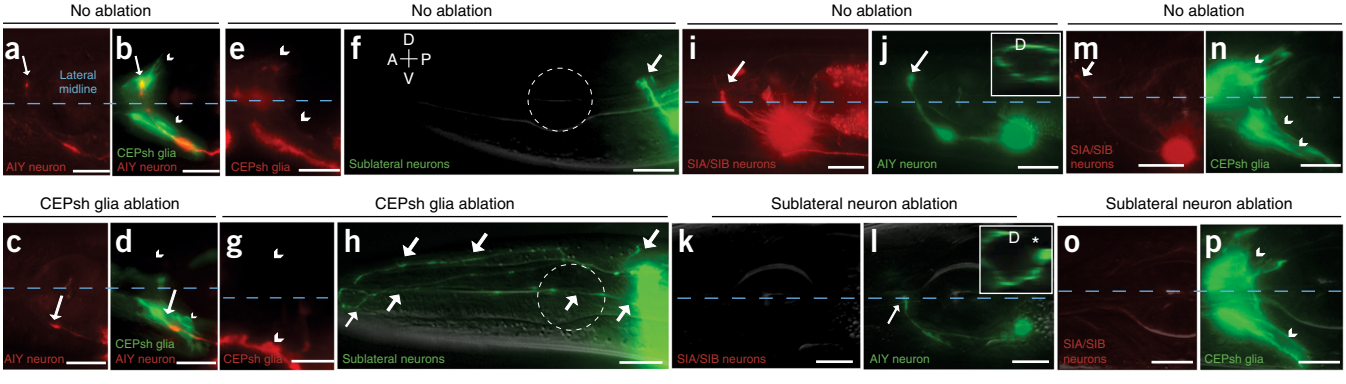

Figure 2 CEPsh glia and SubL axons functionally pioneer the NR. NR entry of AIY follower axons and fasciculation of SubL axons is abnormal in CEPsh-ablated animals. Ablation of SubL neurons results in abnormal AIY NR entry but spares CEPsh membrane growth. (**a**–**d**) *Pttx-3::mCherry*, AIY; *Pmir-228::GFP*, glia. (**e**–**h**) *Pceh-24::GFP*, SIA, SIB, and SMD; *Pptr-10::RFP*, glia. Dotted white outline, first pharyngeal bulb. (**i**–**p**) *Pceh-17::RFP*, SIA and SIB (SIA/SIB); *Pttx-3::GFP*, AIY or *Phlh-17::myristoylated-GFP*, CEPsh glia, both green. Reporter expression patterns are described in Online Methods and in **Supplementary Tables 8** and **10**. Arrow, axon; arrowheads, CEPsh glia; asterisks, NR axon gap. Scale bars, 10 µm.

fewer processes (**Fig. 3i–l** and **Supplementary Movies 1** and **2**): ventral, lateral, and dorsal NR segments spanned >840 nm, >660 nm, and >300 nm, respectively, in the anteroposterior axis in the wild type, but <750 nm, <200 nm, and <150 nm in the mutant. Thus, mutant NR assembly was severely disrupted.

The mutant axon-extension defects were NR-entry specific and did not reflect outgrowth initiation defects. Mutant axons of the tail neuron PVQ had highly penetrant NR entry defects, but they properly extended and navigated along the ventral nerve cord (VNC) before NR entry (**Supplementary Fig. 3a–d**). Furthermore, the VNC and dorsoventral motor neuron commissures, major midbody axon bundles, and positions of neuron and glia cell soma appeared grossly normal in mutants (**Fig. 3e–j**).

Unlike follower neurons, SubL pioneers in the mutant entered the NR but exhibited fasciculation defects reminiscent of CEPsh glia-ablated animals (**Fig. 3m–o**). CEPsh glia morphology, however, appeared unaffected in mutant larvae (**Supplementary Fig. 3k,l**). Therefore, the mutant we identified specifically affected NR entry of various neuronal classes, likely by altering CEPsh glia–pioneer neuron communication.

Genomic and genetic characterization of this mutant revealed, unexpectedly, that two lesions were causal for the highly penetrant NR entry defect. One mutation, *kpc-1*(*ns623*), resulted in a S579T change in the KPC-1 protein, a Kex2/subtilisin-like proprotein convertase homologous to vertebrate Furin. The other mutation, *chin-1*(*ns399*), results in a G273E change in the CHIN-1 protein, a GTPase activating protein (GAP) homologous to vertebrate Chimaerins (**Supplementary Fig. 4a,b**). *kpc-1*(*ns623*) is likely a strong loss-of-function allele, as *kpc-1*(*gk8*) null mutants[25] have similar NR defects when combined with *chin-1*(*ns399*) (**Fig. 3o**). Mutations in the other *C. elegans* proprotein convertases, AEX-5, EGL-3, and BLI-4[26], neither affect AIY axon NR entry nor enhance *chin-1* or *kpc-1* mutant defects (**Supplementary Table 2**). *chin-1*(*ns399*) is likely not a null allele, as homozygous *chin-1*(*tm1909*) deletion is fatal and *chin-1*(*ns399*)/*chin-1*(*tm1909*) transheterozygotes have stronger NR entry defects than *chin-1*(*ns399*) animals (**Fig. 3o**). Our analysis suggests *chin-1*(*ns399*) is a dominant negative allele (see below).

Unlike the highly penetrant NR-entry defects of *kpc-1*;*chin-1* double-mutants, those of *kpc-1* or *chin-1* single mutants are very weak (**Fig. 3o**). Thus, the *kpc-1* and *chin-1* genes are functionally redundant, and the double-mutant *kpc-1*;*chin-1* defines a new class of axon-guidance mutants acting synergistically to assemble the *C. elegans* brain neuropil.

KPC-1 and CHIN-1 function in CEPsh glia and pioneer neurons during NR assembly onset

To uncover the origin of the *kpc-1*;*chin-1* mutant NR defects, we performed time-lapse imaging during NR assembly. AIY or SubL pioneer axons initiated outgrowth at the bean stage of wild-type and *kpc-1*;*chin-1* double-mutant embryos. However, extension into the presumptive NR was delayed in the double-mutant and, occasionally, in *kpc-1* or *chin-1* single mutants (**Fig. 4a–j** and **Supplementary Fig. 5**). Large growth cones were observed in mutant but not wild-type embryos, suggesting that mutant axons were competent for growth cone initiation but navigated slowly (**Fig. 4g**). This is in line with the idea that large growth cones correlate with pausing at choice points[27]. Furthermore, expression of either *kpc-1* or *chin-1* cDNA rescued AIY axon defects of *kpc-1*;*chin-1* mutants only when induced at the end of gastrulation (ball stage: 320 min; **Supplementary Figure 1**) or the bean embryonic stage using a heat-shock-responsive promoter (**Fig. 4k**). Thus, KPC-1 and CHIN-1 are required for proper guidance of axons into the NR before or at the time of pioneer neuron entry.

KPC-1 and CHIN-1 were broadly expressed before and during NR assembly (**Supplementary Fig. 4c,d**), consistent with previous studies[25,28]. However, providing either *kpc-1* or *chin-1* cDNA in all glia or in some SubL neurons partially restored AIY axon NR entry in *kpc-1*;*chin-1* mutants. Moreover, combined cDNA expression in SubL neurons and glia, but not pan-neuronal expression, elicited rescue as efficiently as ubiquitous expression (**Fig. 4l**). Notably, *kpc-1* or *chin-1* cDNA expression in AIY neurons or neighboring GLR cells (**Fig. 1a**) neither rescued AIY axon defects (**Fig. 4l**) nor enhanced the partial rescue obtained by SubL-neuron or glia expression (**Supplementary Table 3**). Furthermore, each cDNA gave partial rescue when driven separately or in combination by *mls-2* or *mir-228* promoters, with overlapping expression in CEPsh, CEPso, OLQsh, OLQso, and ADEsh glia (Online Methods). Non-CEPsh glia are positioned >5–10 µm from the NR during NR formation, and none of their processes are NR-associated[14]. Moreover, mosaic analysis indicated that rescue of AIY axon defects correlated with *kpc-1* or *chin-1* expression in CEPsh glia, but not in AIY, GLRs, muscle, pharynx, or intestine (**Supplementary Table 3**).

Although KPC-1 and CHIN-1 function non-cell-autonomously to guide AIY axons, we wondered whether they function cell-autonomously in SubL neurons. Axon guidance defects of these pioneers are partially rescued by combined KPC-1 and CHIN-1 expression within this commissure, or by glial expression of either KPC-1 or CHIN-1. Yet significantly better rescue is achieved by expressing KPC-1 and CHIN-1 together in glia (**Fig. 4m**).

Together, our data suggest that KPC-1 and CHIN-1 cooperate in CEPsh glia during the onset of NR assembly to guide SubL pioneer neurons. Both proteins function synergistically in glia and SubL neurons to direct follower axons. These results uncover previously unknown roles for Chimaerin and Furin in glia and demonstrate that a specific genetic background can expose the layers of cellular and molecular redundancies controlling NR assembly initiation.

Glia guide pioneer and follower axons using different signals

The synergy of KPC-1 and CHIN-1 on NR assembly suggests that redundant factors guiding NR assembly could be identified by seeking mutations that enhance the weak NR defects of either *kpc-1* or *chin-1* single mutants. Indeed, using candidate-gene approaches, we found that null mutations in *mab-20* (which encodes a *C. elegans* Semaphorin[29]) or *unc-6* (which encodes the only *C. elegans* Netrin[21]) resulted in AIY axon NR entry defects, strongly enhanced by *kpc-1* or *chin-1* lesions (**Fig. 5a**). Disrupting semaphorins SMP-1/2 or SLT-1 (Slit) had no effect on AIY axon NR entry (**Fig. 5a**). Notably, SubL axon navigation was impaired in *unc-6* mutants but not in *mab-20* mutants. UNC-6 expression has been reported in bean-stage CEPsh glia[21]. Moreover, glia expression of UNC-6 could rescue SubL axon guidance defects of *unc-6* mutants (**Fig. 5b**). *mab-20* mRNA was enriched in CEPsh glia (2.5× over all other cells; M. Katz and S.S., personal communication), and we found that *mab-20* cDNA expression of isoform A in embryonic glia, but not SubL neurons, restored AIY axon NR entry (**Fig. 5a**). Thus, both MAB-20 and UNC-6 likely function from glia to regulate NR assembly, through distinct mechanisms of follower- and pioneer-axon navigation. UNC-129 (TGFß), a muscle-secreted UNC-6 regulator[17], also acts in NR assembly through the Netrin pathway: *unc-129* mutations enhanced AIY defects of *mab-20* mutants but not those of *unc-6* mutants (**Fig. 5a**). This result corroborates a role for glial Netrin signaling in NR assembly.

From genetic enhancer screens, in which we mutagenized *kpc-1* or *chin-1* single mutants, we isolated 21 independent strains with robust

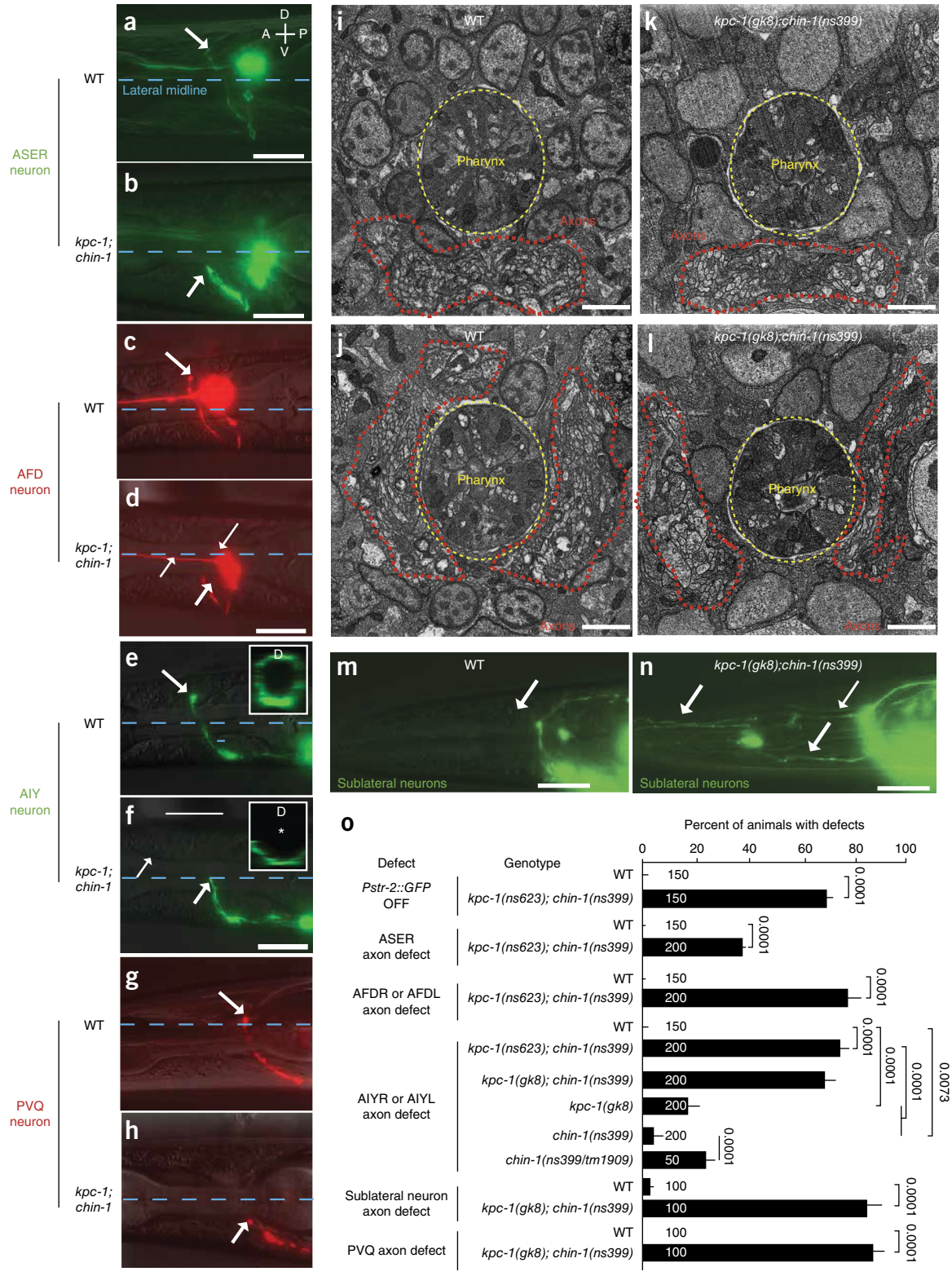

Figure 3 NR axon entry is disrupted in *kpc-1;chin-1* mutants. (**a**–**h**,**m**–**o**) NR guidance of axons of different neuron subtypes and in different commissures is abnormal in *kpc-1;chin-1* mutants. Asterisk, NR axon gap; arrows, dorsal end of NR axon; scale bars, 10 µm. D, dorsal; V, ventral; A, anterior; P, posterior. (**a**,**b**) *Pgcy-5::GFP*. (**c**,**d**) *Pttx-1::RFP*. (**e**,**f**) *Pttx-3::GFP*. Insets, cross-sectional view of AIY axon in the NR. (**b**,**d**,**f**) *kpc-1*(*ns623*);*chin-1*(*ns399*). (**g**,**h**) *Pnpr-11::RFP*. (**i**–**l**) NR structure of L1 animals is abnormal in *kpc-1;chin-1* mutants compared to wild-type animals. Focused ion beam scanning electron microscopy (FIB-SEM) images of wild-type (**i**,**j**) and mutant (**k**,**l**) ventral (**i**,**k**) and lateral (**j**,**l**) NR regions of age-matched L1 animals. Scale bars, 2 µm. Dotted red lines, axons. (**h**,**k**,**l**,**n**) *kpc-1*(*gk8*);*chin-1*(*ns399*). (**m**,**n**,**o**) Fasciculation of SubL neurons is abnormal *kpc-1;chin-1* L1 mutant animals compared to wild-type animals. SubL neurons, *Pceh-24::GFP*. (**a**–**h**,**m**,**n**) Reporter expression patterns are described in Online Methods and **Supplementary Tables 8** and **10**. (**o**) Numbers inside bars, total animals scored per genotype; $n = 4$ independent scoring experiments. Error bars, mean ± s.e.m. Numbers above bars give significant P values from Fisher's exact test; ns, nonsignificant ($P > 0.05$).

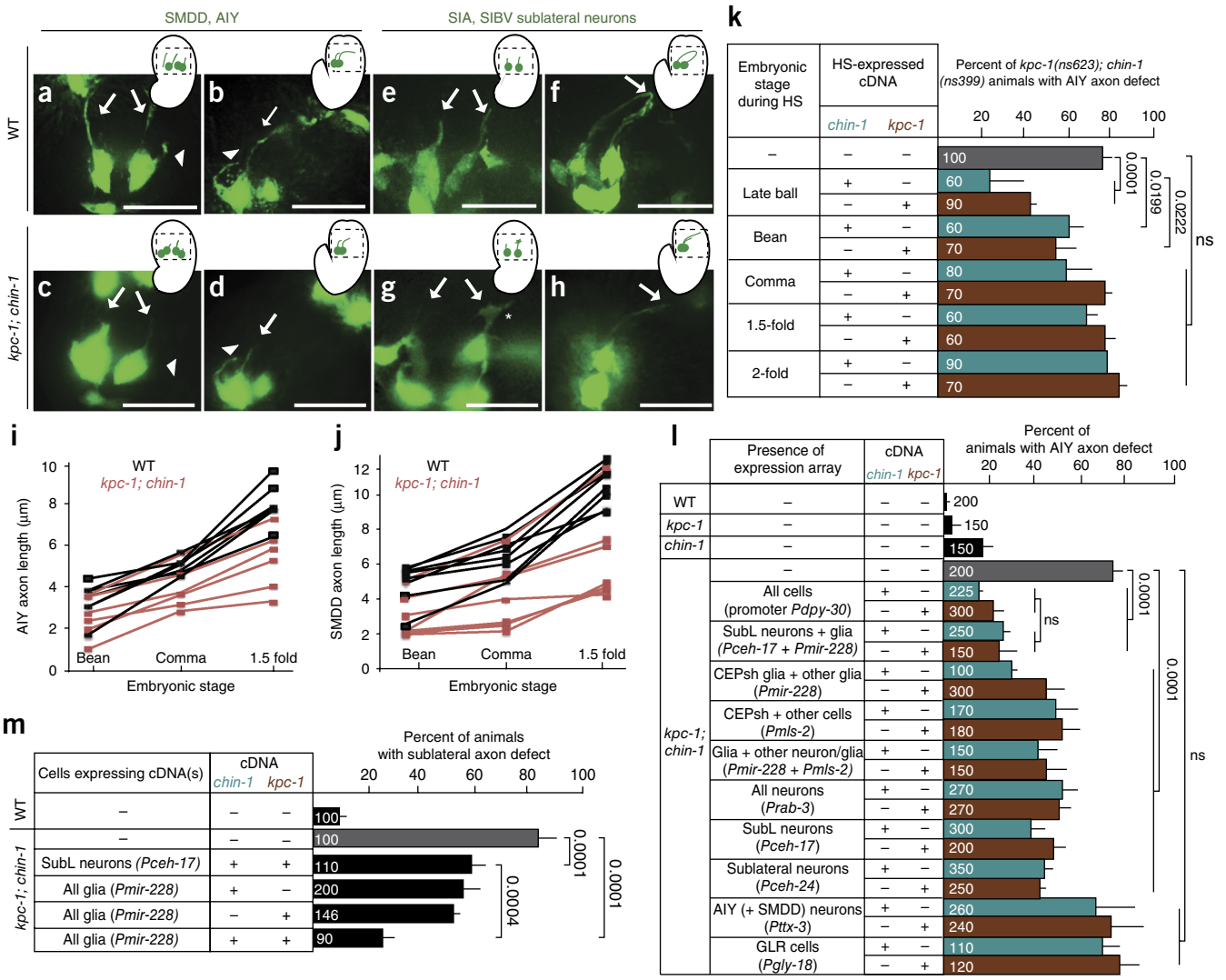

Figure 4 KPC-1 and CHIN-1 act in NR pioneers at the onset of NR assembly. (**a**–**j**) Extension of AIY axons and SubL commissure axons into the presumptive NR is delayed in *kpc-1;chin-1* mutants compared to wild-type embryos. (**a**–**h**) Head region (outlined in schematics) of bean or 1.5-fold embryos expressing *Pttx-3::GFP* (**a**–**d**) or *Pceh-17::GFP* (**e**–**h**). Arrows, SubL axons; arrowheads, AIY axons; asterisk, growth cone. Scale bars, 10 µm. (**i**–**j**) Squares, individual axon measurements at given embryonic stage. Lines track individuals across stages. Numbers of animals analyzed: (**i**) $n = 7$ for WT, $n = 6$ for *chin-1;kpc-1* mutants; (**j**) $n = 8$ for WT, $n = 7$ for *chin-1;kpc-1* mutants. (**k**) CHIN-1 and KPC-1 expression is necessary before the embryonic comma stage for proper NR assembly. HS, heat-shock driving *chin-1* or *kpc-1* cDNA expression. (**l**,**m**) CHIN-1 and KPC-1, acting non-cell-autonomously from SubL neurons and glia, can rescue *chin-1;kpc-1* mutant defects of follower axons. Furthermore, CHIN-1 and KPC-1 acting non-cell-autonomously from glia can rescue *chin-1;kpc-1* mutant defects of pioneer SubL axons. Rescue of mutant defects by cDNA expression using indicated promoters (expression patterns are described in Online Methods and **Supplementary Tables 8** and **10**). The following alleles were used unless otherwise indicated: *kpc-1*(*gk8*) and *chin-1*(*ns399*). (**k**–**m**) Numbers inside bar, total animals scored per genotype; $n = 3$ independent scoring experiments or number of transgenic lines in rescue experiments. Error bars, mean ± s.e.m. Numbers above bars give significant P values from Fisher's exact test; ns, nonsignificant ($P > 0.05$).

AIY-axon NR-entry defects (>60% penetrance). In addition to new *kpc-1* alleles, we isolated three mutations in the gene *fmi-1*, encoding the *C. elegans* Flamingo (CELSR) homolog. These *fmi-1* alleles (*ns701*, *ns717*, and *ns742*; **Supplementary Fig. 6a** and Online Methods) cause weak AIY-axon entry defects on their own and strongly enhance the defective phenotype of the *kpc-1*(*gk8*) mutation (**Fig. 5c**).

FMI-1(CELSR) is a transmembrane protein with extracellular cadherin, EGF, and laminin interaction domains (**Supplementary Fig. 6a**). It is broadly expressed in the *C. elegans* nervous system during embryogenesis and promotes axon fasciculation in the VNC[30], but its role in NR assembly had not been described. *fmi-1* mRNA is enriched in CEPsh glia (13× over all other cells; M. Katz and S.S., personal communication). The previously isolated *fmi-1*(*rh308*) mutation (Q725Ochre) also displayed weak AIY-axon NR-entry defects and strongly enhanced *kpc-1* or *chin-1* mutations (**Fig. 5b**). These defects were fully rescued with genomic DNA (generating three FMI-1 isoforms; **Supplementary Fig. 6a**), as well as with *fmi-1* regulatory sequences fused to isoform A cDNA (**Fig. 5b**). A functional FMI-1-GFP protein partially rescued AIY-axon defects of *fmi-1;chin-1* or *fmi-1;kpc-1* mutants when expressed using glial or SubL neuron promoters. Combined expression of *fmi-1* cDNA in glia and SubL neurons allowed complete rescue, similarly to the rescue achieved by expression under *fmi-1* regulatory sequences. Notably, *fmi-1* or *fmi-1;chin-1* mutants were not defective for SubL-axon fasciculation (**Fig. 5c**).

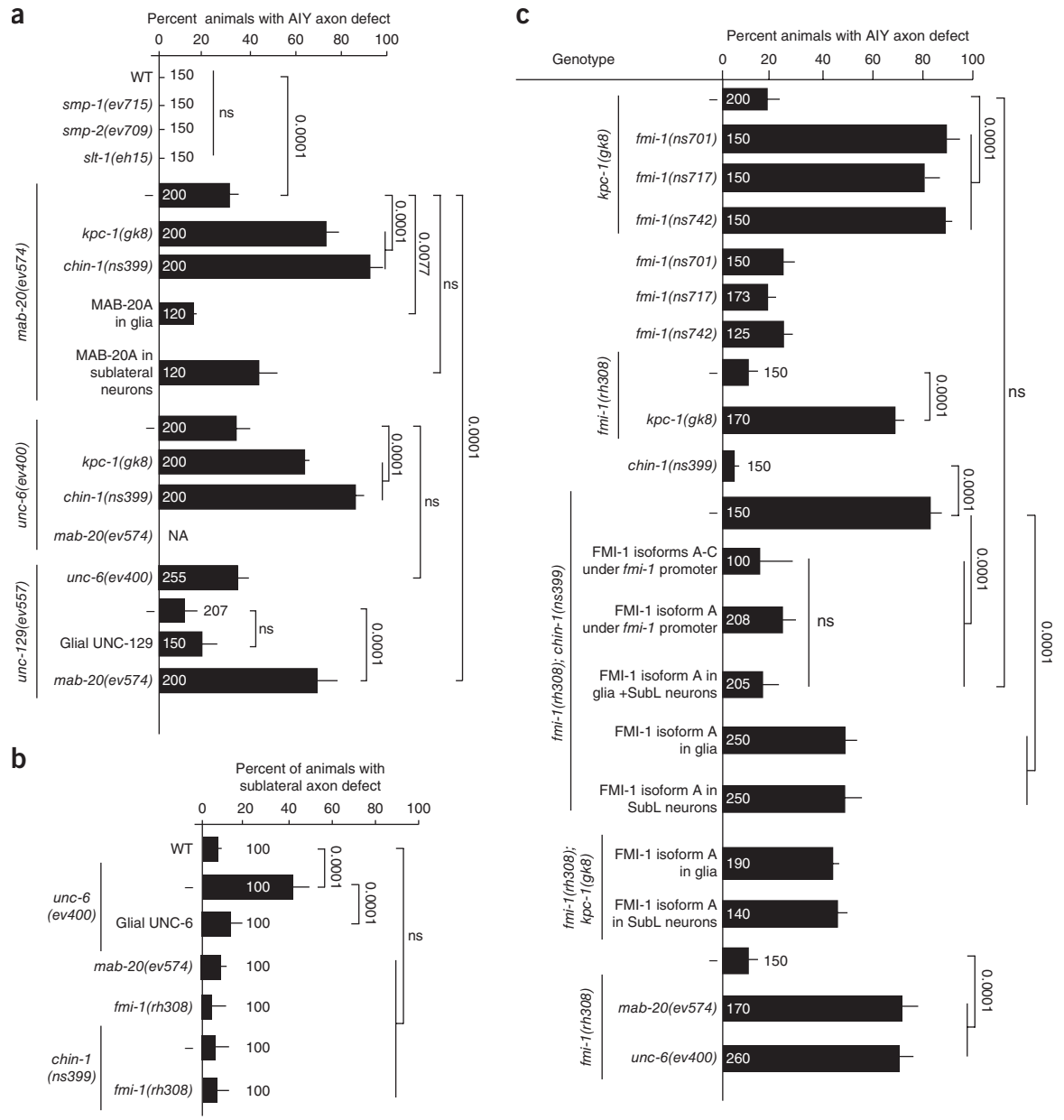

Figure 5 Glia direct pioneer- and follower-axon guidance using distinct signaling pathways. (**a**,**b**) UNC-6 (Netrin) and MAB-20 (Semaphorin) regulate NR assembly. UNC-6 guides primarily pioneer SubL axons while MAB-20 specifically guides follower axons; both act from glia. (**b**,**c**) FMI-1 (Flamingo or CELSR) can act cooperatively from SubL commissure neurons and glia to drive NR assembly by specifically guiding follower axons. (**a**–**c**) cDNA expression of MAB-20, UNC-6, and FMI-1 is driven by *Pmir-228* (glia), *Pceh-17* or *Pceh-24* (SubL neurons), or endogenous regulatory regions. Expression patterns are described in Online Methods and **Supplementary Tables 8** and **10**. Numbers inside bars, total animals scored per genotype, $n = 4$ independent scoring experiments on nontransgenic mutant populations or n = number of transgenic lines in rescue experiments. Error bars, mean ± s.e.m. Numbers above bars, P values from Fisher's exact test; ns, nonsignificant ($P > 0.05$).

Thus, FMI-1, together with KPC-1 and/or CHIN-1, promotes follower axon guidance during NR assembly and acts from SubL neurons and glia, an unexpected result given that other CELSR homologs had been previously suggested to function only from neurons[31,32].

Overall, glia appear to differentially guide pioneer and follower axons. Glial UNC-6 (Netrin) controls pioneer-axon guidance, which can affect follower-axon extension, while MAB-20 (Semaphorin) and FMI-1 (CELSR) act in glia for follower-axon and not pioneer-axon guidance (see also below).

KPC-1 and CHIN-1 control glial guidance-cue trafficking

To understand how *kpc-1* and *chin-1* affect NR axon guidance, we examined FMI-1-GFP subcellular localization. FMI-1-GFP localized to the NR bundle of 1.5-fold wild-type embryos (**Fig. 6a**,**b**). In *kpc-1;chin-1* double-mutants and in *kpc-1* or *chin-1* single mutants, however, GFP was detected more strongly outside the NR in cell bodies, dendrites, and proximal axon segments (**Fig. 6c**–**e** and **Supplementary Fig. 7**). FMI-1-GFP mislocalization is unlikely to be a result of axon morphology defects, as similar mislocalization occurred in *chin-1* and

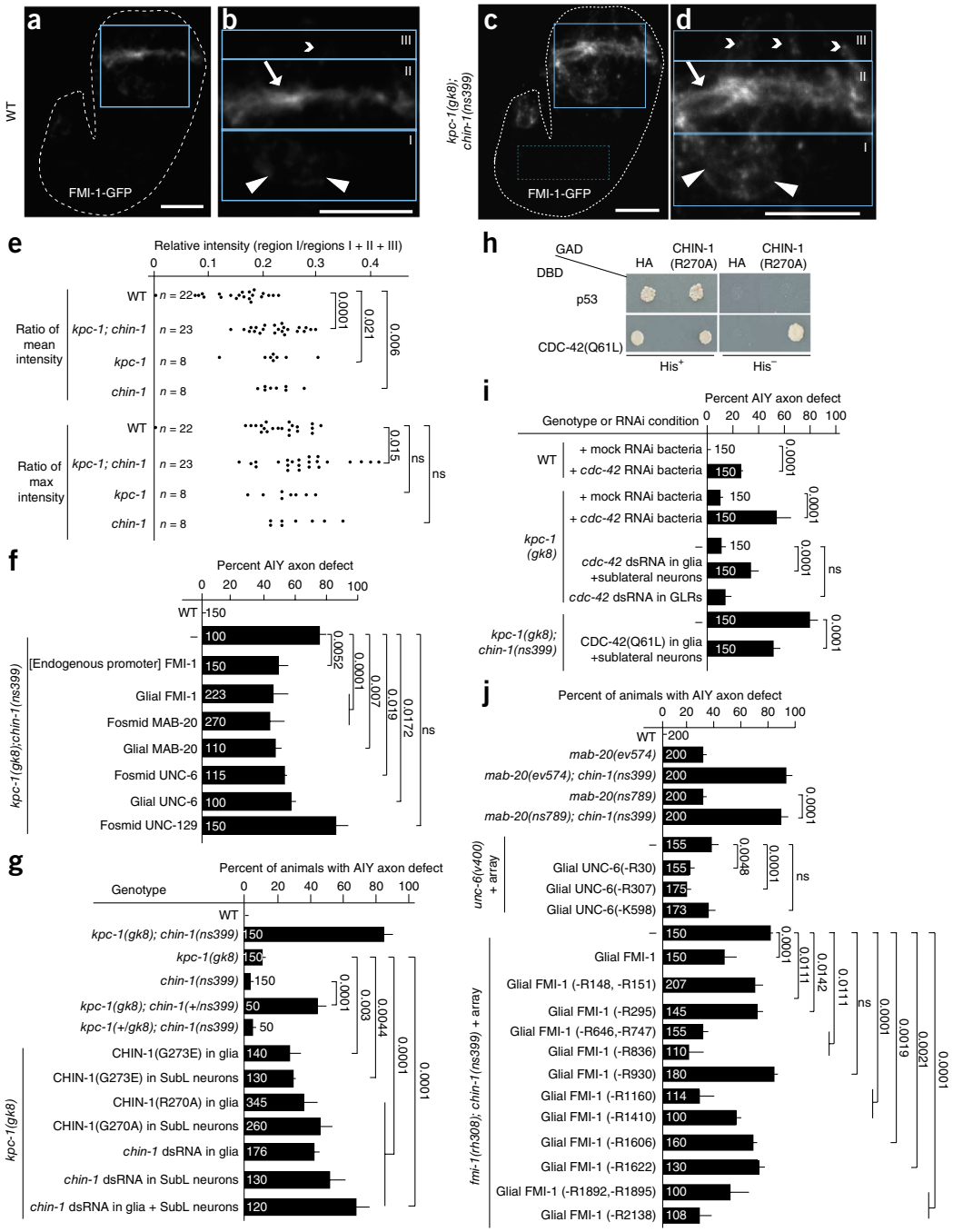

Figure 6 KPC-1 and CHIN-1 control guidance-cue trafficking. (**a**–**e**) FMI-1-GFP localizes to the NR bundle of 1.5-fold wild-type embryos but is detected abnormally outside the NR in *kpc-1;chin-1* mutants. (**a**,**c**) 1.5-fold embryos expressing *Pfmi-1::FMI-1-GFP* and (**b**,**d**) magnified view of their head regions. Blue boxes outline regions of interest I (cell bodies, triangles), II (NR, arrows), and III (dendrites, arrowheads). Scale bars, 10 µm. (**e**) FMI-1-GFP ectopic signal is quantified as described in Online Methods (see also **Supplementary Fig. 7**). Number of animals analyzed appears in the graph (*n*). Numbers above bars give significant *P* values from *t* test test (GraphPad); ns, nonsignificant ($P > 0.05$). *t* ratios for group comparisons of wild-type and *kpc-1;chin-1*, wild-type and *kpc-1*, and wild-type and *chin-1* are 4.95, 2.44, and 2.95, respectively, for mean intensity ratio; and 2.55, 0.74, and 1.50, respectively, for max intensity ratio. Number of degrees of freedom equals the number of pairs minus 1. (**f**) Overexpression of UNC-6, MAB-20, and FMI-1, but not UNC-129, can partially restore the AIY axon defects of *kpc-1;chin-1* mutant animals. (**g**) *chin-1*(*ns399*) encodes a dominant-negative protein functionally similar to CHIN-1 variants harboring an Arginine finger-mutation. (**h**) CHIN-1 specifically binds CDC-42 in yeast-two-hybrid assays. p53-DBD and HA-GAD, negative controls; CDC-42(Q61L)-DBD and CHIN-1(R270A)-GAD, positive interactors. (**i**) *cdc-42* RNAi results in abnormal AIY-axon NR entry. Mock RNAi, L4440 vector. (**j**) MAB-20, UNC-6, and FMI-1 predicted furin motifs are important for AIY axon NR entry. (**f**,**g**,**i**,**j**) cDNA expression is driven by *Pmir-228* (glia), *Pceh-17* (SubL neurons), *Pgly-18* (GLR cells), or endogenous regulatory regions (Online Methods). (**j**) *mab-20*(*ns789*), CRISPR allele. (-Rn) or (-Kn): extrachromosomal array of *unc-6* or *fmi-1* cDNA with single amino-acid deletions perturbing predicted Furin-recognition motifs (**Supplementary Fig. 6** and **Supplementary Table 5**). Numbers inside bars, total animals scored per genotype ($n = 4$ independent scoring experiments) or number of transgenic lines in rescue experiments. Error bars, mean ± s.e.m. Numbers above bars, exact *P* values by Fisher's exact test; ns, nonsignificant ($P > 0.05$).

kpc-1 single mutants, yet these animals had largely normal neuron structures (**Fig. 3o** and **Supplementary Fig. 5c**,**d**). Thus, KPC-1 and CHIN-1 are required for NR trafficking of FMI-1 (Flamingo). This suggests a previously unknown function for Chimaerins in trafficking and sheds light on how CELSR proteins are localized.

The partial mislocalization of FMI-1-GFP, as well as the incompletely penetrant defects of the *kpc-1;chin-1* double-mutant, suggests that some trafficking of guidance cues does occur in this strain. If so, then overexpression of guidance cues, allowing more guidance factors to be trafficked, should partially rescue *kpc-1;chin-1* double-mutants. Indeed, we found that AIY NR entry in *kpc-1;chin-1* mutants was partially restored by overexpression of FMI-1, MAB-20, or UNC-6 using endogenous or glia-specific regulatory sequences (**Fig. 6f**). This suggests that trafficking of MAB-20 and UNC-6 from glia may also require KPC-1 and CHIN-1. By contrast, *kpc-1;chin-1* mutants were not rescued by overexpression of UNC-129 (**Fig. 6f**). UNC-129 does not act in glia, as its expression in glia did not rescue *unc-129* mutant NR defects (**Fig. 5a**). Thus, its inability to rescue *kpc-1;chin-1* mutants under its endogenous promoter supports the specificity of our glial overexpression assay; and, contrary to previous studies[33], CHIN-1 acts upstream, not downstream, of guidance cues for NR assembly.

In summary, KPC-1 and CHIN-1 function upstream of at least three redundant guidance factors acting specifically in glia (MAB-20, UNC-6) or cooperatively in glia and SubL pioneers (FMI-1) to control NR assembly. These guidance factors also regulate amphid-commissure follower-axon navigation in addition to AIY-axon NR-entry (**Supplementary Table 4**).

CHIN-1 (Chimaerin) functions with CDC-42 (GTPase)

To understand CHIN-1 function, we characterized the *chin-1*(*ns399*) mutation. This G273E substitution affects a conserved Arginine finger motif (ArgF, R270), mutations in which allow GTPase binding but not hydrolytic activity[34]. We found that NR axon-entry defects in *kpc-1*(*null*) mutants were enhanced by a heterozygous *chin-1*(*ns399*)/+ lesion (**Fig. 6g**). Glia or SubL-neuron overexpression of CHIN-1(G273E) or CHIN-1(R270A) had similar effects, as did reduction of *chin-1* gene function using a hairpin-RNAi in embryonic glia, SubL neurons, or both (**Fig. 6g**). Therefore, *chin-1*(*ns399*) is a dominant-negative allele that may block activity of small GTPases.

Through a candidate yeast-two-hybrid screen (Online Methods), we identified CDC-42 as a major CHIN-1 interactor (**Fig. 6h**). Chimaerins bind CDC42 and modulate its GTPase activity[35], and CDC42 can regulate trafficking[36]. NR axon-entry defects of follower AIY axons in *kpc-1*(*null*) mutants were strongly enhanced by RNAi induced by bacteria-fed *cdc-42* dsRNA or by expression of a *cdc-42* hairpin in glia and SubL neurons but not in neighboring GLR cells (**Fig. 6i**). This suggests that CDC-42 functions non-cell-autonomously from glia and SubL neurons for follower axon guidance. Given that CHIN-1(G273E) likely represents a dominant-negative GTPase-activating protein, we reasoned that expression of a constitutively active CDC-42(Q61L) could sequester dominant-negative CHIN-1(G273E), allowing endogenous CDC-42 to bind downstream effectors. In line with this model, expression of CDC-42(Q61L) in NR pioneers partially rescued AIY axon NR defects of *kpc-1;chin-1* mutants (**Fig. 6i**). Thus, CHIN-1 acts through the Rho-family GTPase CDC-42 to control NR assembly.

Predicted KPC-1 (Furin) cleavage sites in glial guidance cues are required for NR assembly

Furins are implicated in secretory-pathway trafficking[37] as well as in Semaphorin and cadherin processing[38,39]. We identified putative Furin cleavage sites in MAB-20 (Semaphorin), UNC-6 (Netrin), and FMI-1 (Flamingo) proteins using an RXXR consensus motif or using cleavage sites predicted by the ProP1.0 algorithm (**Supplementary Fig. 6a–c**, **Supplementary Table 5**, and Online Methods). A single predicted site in MAB-20 fulfills both criteria and is conserved in vertebrate Semaphorin homologs. Mutation of the conserved arginine (R247H) using CRISPR–Cas9 resulted in AIY axon defects similar to those of *mab-20*(*ev574*)-null mutants and enhanced defects of single *chin-1* mutants (**Fig. 6j**). The ProP1.0 algorithm also identified three predicted motifs in the UNC-6 (Netrin) protein that were not conserved and did not conform to the RXXR consensus. *unc-6* proteins expressed in glia and carrying R30 or R37, but not K598, lesions could rescue AIY entry-defects of *unc-6* mutants (**Fig. 6**, **Supplementary Fig. 6**, and **Supplementary Table 5**).

FMI-1 has 15 predicted furin motifs: six are ProP1.0-predicted cleavage sites not conforming to the RXXR consensus and nine are RXXR motifs (**Supplementary Fig. 6** and **Supplementary Table 5**). None of these are highly conserved. Nonetheless, *fmi-1* cDNAs altering amino acids R151, R295, R930, R1410, R1606, or R1622 did not robustly rescue AIY NR-entry defects in *fmi-1;chin-1* mutants (**Fig. 6j**). Thus, these MAB-20-, UNC-6-, and FMI-1-predicted furin motifs, likely recognized by KPC-1, are important *in vivo* for NR assembly.

DISCUSSION

Our studies support a model for hierarchical assembly of the *C. elegans* NR (**Supplementary Fig. 8**). At the onset of embryonic morphogenesis, axons of SubL neurons fasciculate and navigate anteriorly toward ventral CEPsh glia. Dorsally directed processes of these glia may define a turning point for SubL axons, which coalesce with glial processes to define the NR tract. Based on our EM studies, NR pioneer bundles may contain 2–4 additional processes that we have not yet identified. These may include axons and/or processes of the CEPshD glia. The two dorsal CEPsh glia extend ventrally directed processes enveloping the adult NR. Although tracking individual CEPshD processes was challenging, these processes are present before late morphogenesis and their presence is functionally important for follower- and pioneer-axon guidance (**Fig. 2**).

CEPsh glia drive SubL axon navigation and then cooperate with these pioneer neurons to promote NR entry of follower axons, which otherwise do not enter the NR properly and instead either stop or grow ectopically. This synergy is mediated by glia-secreted UNC-6 (Netrin), likely acting primarily for pioneer-axon guidance, and by glia-secreted MAB-20 (Semaphorin), acting specifically for follower-axon guidance. The fasciculation protein FMI-1 (CELSR) acts from glia and SubL neurons, perhaps creating a common guidance substrate that then directs follower axons. Follower axons enter the NR at different times and do so independently or in commissures that build over time.

SubL pioneer neurons have unique characteristics: we demonstrate that they have CEPsh-glia-independent growth potential, unlike follower neurons, and form the earliest fasciculating commissure entering the NR. These neurons are important for follower-axon NR entry and have previously been implicated in NR positioning[20]. The NR guidance and positioning activities might reflect distinct temporal roles for SubL commissure components. Adult anatomical studies reveal that SubL neurons occupy central neuropil positions and are sparsely connected. Indeed, SIA and SIB may exhibit no chemical synaptic output onto other NR neurons[16] (*C. elegans* Neural Network wormweb, http://wormweb.org/neuralnet). Thus, NR pioneers represent a distinct neuronal class. Moreover, within the SubL fascicle, SIA and SIB neurons were sufficient for mutant rescue, as these are

the neurons common to the two different drivers we used (**Fig. 4i** and **Supplementary Tables 3** and **10**), and they appear to grow slightly earlier than SMD neurons (**Fig. 1f** and **Supplementary Fig. 2b–d**), suggesting that these may be the key components of the SubL bundle.

Our studies also suggest that molecular and cellular redundancies may have previously hindered identification of NR assembly cues. Key to our dissection of the process was the identification of the *kpc-1*;*chin-1* double-mutant, which revealed a bottleneck that we used to expose the activities of multiple guidance factors. Notably, while KPC-1 (Furin) and CHIN-1 (Chimaerin) are broadly expressed and are implicated in many cellular processes[25,28,40], the dominant-negative *chin-1* mutation we uncovered, when accompanied by *kpc-1*-null lesions, has remarkably specific synergy in NR assembly. We suggest that a similar mutant combination may uncover novel guidance molecules and interactions in other organisms as well.

Our studies also provide new insights into Chimaerin and Furin functions in the nervous system. Furins are known to cleave guidance cues[38,41]; however, functional evidence of roles for these proteases in glia are not well-documented. Murine β2-Chimaerin mediates Sema3F-dependent axon pruning[42] while human α2-chimaerin mutations cause Duane's retraction syndrome 2, and the protein has been suggested to act cell-autonomously in neurons, downstream of a Semaphorin–Plexin pathway for oculomotor nerve guidance[33]. Notably, however, loss of murine α2-chimaerin causes aberrant axon midline crossing[11], and dominant α2-chimaerin lesions cause axon stalling and defasciculation[43]. The similarities between these abnormalities and the NR defects we observe raise the possibility that CHIN-1 may function non-cell-autonomously upstream of guidance cues in pioneer neurons and/or glia in vertebrates as well.

We reveal key roles for *C. elegans* CEPsh glia in regulating NR assembly. Although CEPsh glia have not been demonstrated to be neural progenitors like vertebrate radial glia[44], our work, nonetheless, suggests similarities between these cells in their development, gene expression, and roles in CNS formation. Like embryonic CEPsh glia, vertebrate radial glia extend thin bipolar processes that associate early in development with neurons and demarcate CNS domains[45]. In vertebrates, radial glia of the optic tectum express Semaphorins and Furin[41,46], as do CEPsh glia, and they may be the first source of Netrin1 expression in the embryonic telencephalon[47]. Notably, radial glia pial processes were recently reported to be the functionally relevant sites of Netrin1 activity during commissural-axon guidance in the vertebrate spinal cord[48,49]. The same guidance molecule in embryonic CEPsh glia drives NR pioneer-neuron guidance. Finally, radial glia morphologically transform into astrocytes, glial cells with elaborate membranes that extend fine projections approximating synapses[44,50]. Similarly, embryonic CEPsh glia develop into adult CEPsh glia, which resemble astrocytes in morphology (**Fig. 1**), in molecular composition (M. Katz and S.S., personal communication) and in proximity to synapses[16]. These similarities between *C. elegans* CEPsh glia and vertebrate radial glia and astrocytes are remarkable, as these animals last shared an ancestor over a billion years ago. Therefore, our studies suggest that radial glia may play key roles in pioneering brain assembly by guiding pioneer axons in vertebrates as well.

METHODS

Methods, including statements of data availability and any associated accession codes and references, are available in the online version of the paper.

Note: Any Supplementary Information and Source Data files are available in the online version of the paper.

ACKNOWLEDGMENTS

We thank C. Bargmann, V. Bertrand, L. Cochella, L. Chen, J. Culotti, O. Hobert, H. Hutter, L. Kutscher, J. Malin, G. Oikonomou, N. Pujol, P. Sengupta, B. Tursun, WG. Wadsworth, S. Wallace, and M. Zhen for reagents, as well as M. Katz for sharing unpublished information. Some strains were provided by the CGC, funded by NIH (P40 OD010440). We thank the Rockefeller University Bio-Imaging and Electron Microscopy Resource Centers for technical help, W.J. Rice at the Simons Electron Microscopy Center (NYSBC) for help with FIB-SEM imaging, and C. Bargmann and the Shaham lab for insights. G.R. was supported by a Shelby White and Leon Levy Foundation fellowship. This work was supported in part by NIH grants NS064273 and NS073121 to S.S.

AUTHOR CONTRIBUTIONS

G.R. performed all experiments except the electron microscopy studies, which were performed by Y.L. C.L. and A.S. assisted with generation of plasmids, strains and yeast-two-hybrid screens. S.S. supervised the project. G.R and S.S. wrote the manuscript.

COMPETING FINANCIAL INTERESTS

The authors declare no competing financial interests.

1. Easter, S.S. Jr., Ross, L.S. & Frankfurter, A. Initial tract formation in the mouse brain. *J. Neurosci.* **13**, 285–299 (1993).
2. Chédotal, A. & Richards, L.J. Wiring the brain: the biology of neuronal guidance. *Cold Spring Harb. Perspect. Biol.* **2**, a001917 (2010).
3. Jacobs, J.R., Goodman, C.S. & Ii, C.N.S. Embryonic development of axon pathways in the Drosophila CNS. II. Behavior of pioneer growth cones. *J. Neurosci.* **9**, 2412–2422 (1989).
4. Hidalgo, A., Urban, J. & Brand, A.H. Targeted ablation of glia disrupts axon tract formation in the Drosophila CNS. *Development* **121**, 3703–3712 (1995).
5. Hidalgo, A. & Booth, G.E. Glia dictate pioneer axon trajectories in the Drosophila embryonic CNS. *Development* **127**, 393–402 (2000).
6. Whitington, P.M., Quilkey, C. & Sink, H. Necessity and redundancy of guidepost cells in the embryonic *Drosophila* CNS. *Int. J. Dev. Neurosci.* **22**, 157–163 (2004).
7. Takizawa, K. & Hotta, Y. Pathfinding analysis in a glia-less *gcm* mutant in Drosophila. *Dev. Genes Evol.* **211**, 30–36 (2001).
8. Placzek, M. & Briscoe, J. The floor plate: multiple cells, multiple signals. *Nat. Rev. Neurosci.* **6**, 230–240 (2005).
9. Minocha, S. *et al.* Nkx2.1-derived astrocytes and neurons together with Slit2 are indispensable for anterior commissure formation. *Nat. Commun.* **6**, 6887 (2015).
10. Kolodkin, A.L. & Tessier-Lavigne, M. Mechanisms and molecules of neuronal wiring: a primer. *Cold Spring Harb. Perspect. Biol.* **3**, a001727 (2011).
11. Iwasato, T. *et al.* Rac-GAP α-chimerin regulates motor-circuit formation as a key mediator of EphrinB3/EphA4 forward signaling. *Cell* **130**, 742–753 (2007).
12. Jaworski, A. *et al.* Operational redundancy in axon guidance through the multifunctional receptor Robo3 and its ligand NELL2. *Science* **350**, 961–965 (2015).
13. Jorgensen, E.M. & Mango, S.E. The art and design of genetic screens: *caenorhabditis elegans*. *Nat. Rev. Genet.* **3**, 356–369 (2002).
14. Sulston, J.E., Schierenberg, E., White, J.G. & Thomson, J.N. The embryonic cell lineage of the nematode *Caenorhabditis elegans*. *Dev. Biol.* **100**, 64–119 (1983).
15. Oikonomou, G. & Shaham, S. The glia of *Caenorhabditis elegans*. *Glia* **59**, 1253–1263 (2011).
16. White, J.G., Southgate, E., Thomson, J.N. & Brenner, S. The structure of the nervous system of the nematode *Caenorhabditis elegans*. *Phil. Trans. R. Soc. Lond. B* **314**, 1–340 (1986).
17. MacNeil, L.T., Hardy, W.R., Pawson, T., Wrana, J.L. & Culotti, J.G. UNC-129 regulates the balance between UNC-40 dependent and independent UNC-5 signaling pathways. *Nat. Neurosci.* **12**, 150–155 (2009).
18. Zallen, J.A., Kirch, S.A. & Bargmann, C.I. Genes required for axon pathfinding and extension in the *C. elegans* nerve ring. *Development* **126**, 3679–3692 (1999).
19. Hedgecock, E.M., Culotti, J.G. & Hall, D.H. The *unc-5*, *unc-6*, and *unc-40* genes guide circumferential migrations of pioneer axons and mesodermal cells on the epidermis in *C. elegans*. *Neuron* **4**, 61–85 (1990).
20. Kennerdell, J.R., Fetter, R.D. & Bargmann, C.I. Wnt-Ror signaling to SIA and SIB neurons directs anterior axon guidance and nerve ring placement in *C. elegans*. *Development* **136**, 3801–3810 (2009).
21. Wadsworth, W.G., Bhatt, H. & Hedgecock, E.M. Neuroglia and pioneer neurons express UNC-6 to provide global and local netrin cues for guiding migrations in *C. elegans*. *Neuron* **16**, 35–46 (1996).
22. Durbin, R.M. *Studies on the development and organisation of the nervous system of Caenorhabditis elegans*. PhD dissertation, Cambridge Univ. (1987).
23. Yoshimura, S., Murray, J.I., Lu, Y., Waterston, R.H. & Shaham, S. mls-2 and vab-3 control glia development, hlh-17/Olig expression and glia-dependent neurite extension in *C. elegans*. *Development* **135**, 2263–2275 (2008).

24. Troemel, E.R., Sagasti, A. & Bargmann, C.I. Lateral signaling mediated by axon contact and calcium entry regulates asymmetric odorant receptor expression in *C. elegans*. *Cell* **99**, 387–398 (1999).
25. Schroeder, N.E. *et al*. Dauer-specific dendrite arborization in *C. elegans* is regulated by KPC-1/Furin. *Curr. Biol.* **23**, 1527–1535 (2013).
26. Thacker, C. & Rose, A.M. A look at the *Caenorhabditis elegans* Kex2/Subtilisin-like proprotein convertase family. *BioEssays* **22**, 545–553 (2000).
27. Mason, C. & Erskine, L. Growth cone form, behavior, and interactions in vivo: retinal axon pathfinding as a model. *J. Neurobiol.* **44**, 260–270 (2000).
28. Kumfer, K.T. *et al*. CGEF-1 and CHIN-1 regulate CDC-42 activity during asymmetric division in the *Caenorhabditis elegans* embryo. *Mol. Biol. Cell* **21**, 266–277 (2010).
29. Roy, P.J., Zheng, H., Warren, C.E. & Culotti, J.G. *mab-20* encodes Semaphorin-2a and is required to prevent ectopic cell contacts during epidermal morphogenesis in *Caenorhabditis elegans*. *Development* **127**, 755–767 (2000).
30. Steimel, A. *et al*. The Flamingo ortholog FMI-1 controls pioneer-dependent navigation of follower axons in *C. elegans*. *Development* **137**, 3663–3673 (2010).
31. Organisti, C., Hein, I., Grunwald Kadow, I.C. & Suzuki, T. Flamingo, a seven-pass transmembrane cadherin, cooperates with Netrin/Frazzled in Drosophila midline guidance. *Genes Cells* **20**, 50–67. http://dx.doi.org/10.1111/gtc.12202 (2015).
32. Feng, J. *et al*. Celsr3 and Fzd3 organize a pioneer neuron scaffold to steer growing thalamocortical axons. *Cereb. Cortex* **26**, 3323–3334 (2016).
33. Ferrario, J.E. *et al*. Axon guidance in the developing ocular motor system and Duane retraction syndrome depends on Semaphorin signaling via alpha2-chimaerin. *Proc. Natl. Acad. Sci. USA* **109**, 14669–14674 (2012).
34. Pan, X., Eathiraj, S., Munson, M. & Lambright, D.G. TBC-domain GAPs for Rab GTPases accelerate GTP hydrolysis by a dual-finger mechanism. *Nature* **442**, 303–306 (2006).
35. Chen, W., Lim, H.H. & Lim, L. The CDC42 homologue from *Caenorhabditis elegans*. Complementation of yeast mutation. *J. Biol. Chem.* **268**, 13280–13285 (1993).
36. Lipschutz, J.H. & Mostov, K.E. Exocytosis: the many masters of the exocyst. *Curr. Biol.* **12**, R212–R214 (2002).
37. Hosaka, M. *et al*. Arg-X-Lys/Arg-Arg motif as a signal for precursor cleavage catalyzed by furin within the constitutive secretory pathway. *J. Biol. Chem.* **266**, 12127–12130 (1991).
38. Adams, R.H., Lohrum, M., Klostermann, A., Betz, H. & Püschel, A.W. The chemorepulsive activity of secreted semaphorins is regulated by furin-dependent proteolytic processing. *EMBO J.* **16**, 6077–6086 (1997).
39. Sadeqzadeh, E. *et al*. Furin processing dictates ectodomain shedding of human FAT1 cadherin. *Exp. Cell Res.* **323**, 41–55 (2014).
40. Hung, W.L., Wang, Y., Chitturi, J. & Zhen, M. A *Caenorhabditis elegans* developmental decision requires insulin signaling-mediated neuron-intestine communication. *Development* **141**, 1767–1779 (2014).
41. Tassew, N.G., Charish, J., Seidah, N.G. & Monnier, P.P. SKI-1 and Furin generate multiple RGMa fragments that regulate axonal growth. *Dev. Cell* **22**, 391–402 (2012).
42. Riccomagno, M.M. *et al*. The RacGAP β2-Chimaerin selectively mediates axonal pruning in the hippocampus. *Cell* **149**, 1594–1606 (2012).
43. Miyake, N. *et al*. Human *CHN1* mutations hyperactivate alpha2-chimaerin and cause Duane's retraction syndrome. *Science* **321**, 839–843 (2008).
44. Barry, D.S., Pakan, J.M.P. & McDermott, K.W. Radial glial cells: key organisers in CNS development. *Int. J. Biochem. Cell Biol.* **46**, 76–79 (2014).
45. Rakic, P. Neuron-glia relationship during granule cell migration in developing cerebellar cortex. A Golgi and electronmicroscopic study in *Macacusrhesus*. *J. Comp. Neurol.* **141**, 283–312 (1971).
46. Kuwajima, T. *et al*. Optic chiasm presentation of Semaphorin6D in the context of Plexin-A1 and Nr-CAM promotes retinal axon midline crossing. *Neuron* **74**, 676–690 (2012).
47. Métin, C., Deléglise, D., Serafini, T., Kennedy, T.E. & Tessier-Lavigne, M. A role for netrin-1 in the guidance of cortical efferents. *Development* **124**, 5063–5074 (1997).
48. Dominici, C. *et al*. Floor-plate-derived netrin-1 is dispensable for commissural axon guidance. *Nature* **545**, 350–354 (2017).
49. Varadarajan, S.G. *et al*. Netrin1 produced by neural progenitors, not floor plate cells, is required for axon guidance in the spinal cord. *Neuron* **94**, 790–799 e3 (2017).
50. Voigt, T. Development of glial cells in the cerebral wall of ferrets: direct tracing of their transformation from radial glia into astrocytes. *J. Comp. Neurol.* **289**, 74–88 (1989).

ONLINE METHODS

C. elegans methods. *C. elegans* were cultured as previously described[51,52]. We used Bristol N2 strain the wild type, and raised animals at 20 °C (unless otherwise indicated) for at least two generations under *ad libitum* feeding conditions. Animals used for phenotypic analysis were hermaphrodites (not males). The age of animals analyzed is indicated in individual sections of the methods presenting of phenotypic scoring and imaging.

Integration of extrachromosomal arrays was performed using UV with trioxalen (Sigma, T6137). Germline transformations to generate unstable extrachromosomal arrays (transgenes) were performed using standard protocols of microinjection[53].

Strains and plasmids used in this study. *Previously published mutant strains used in this study.* Some strains (listed below) were provided from the CGC, funded by the NIH Office of Research Infrastructure Programs (P40 OD010440) and by the National BioResource Project (NBRP, Japan).

The following previously published mutant alleles were used in this study:

- LG.I *kpc-1*(*gk8*), *bli-4*(*e937*), *aex-5* (*gk419962*), and *mab-20*(*ev574*)
- LG.III: *chin*(*tm1909*/+)
- LG.IV: *ced-3*(*n717*) and *unc-129*(*ev557*)
- LG.V: *egl-3*(*n150*) and *fmi-1*(*rh308*) and
- LG.X: *lin-15*(*n765*) and *unc-6*(*ev400*) *X*

New mutant alleles generated in this study. Information is provided in **Supplementary Table 6**.

Transgenic strains and plasmids used in this study. Information on unstable extrachromosomal transgenes and stably integrated transgenes respectively is provided in **Supplementary Tables 7** and **8**, respectively.

List of plasmids used in this study. Information is provided in **Supplementary Table 9**. DNA sequences of pGR plasmids (generated in this study) are available upon request.

Expression patterns of reporters used in this study. Suitable markers were identified by screening transcription-factor, cell-differentiation, and neuropeptide gene reporters. Markers suitable for process-imaging in the bean and subsequent embryonic stages were selected based on the pattern reported in previous publications and the criterion of sparse expression, allowing us to easily establish cell identities and track early processes. The pattern was confirmed in this study using embryonic imaging and cell identification was based on cell morphology (axon–dendrite pattern) and cell positioning as previously defined[14,54,55], and using the resources of Wormatlas (http://www.wormatlas.org). Data on the expression patterns of reporters used is provided in **Supplementary Table 10**.

Isolation of mutants and genetic mapping. Animals were mutagenized using 70 mM ethyl methanesulfonate (EMS, Sigma) at 20 °C for 4 h.

Primary screen. ntIs1;*kyIs136* animals were mutagenized, nonclonal F2 progeny were examined on a Zeiss Axioplan 2 fluorescence microscope (with 63×/1.4 NA objective and FITCH/GFP filter set (Chroma, Set 51019), and animals with aberrant AWC and ASE axon morphologies were recovered.

Secondary enhancer screens. Kpc-1(*gk8*)*;mgIs18* or *chin-1*(*ns399*)*;mgIs18* animals were mutagenized, nonclonal F2 progeny were examined on a dissecting GFP scope, and animals with defective AIY NR axon were isolated as enhancer candidates. True double-mutant enhancers were identified with AIY axon defects of penetrance >60%. DNA samples from mutants were prepared and whole genome sequencing (WGS) was performed at the Genomics Resource Center at The Rockefeller University. Mutated loci were identified using SNP mapping and using rescue experiments with fosmids or plasmid vectors.

Mapping. Mutant animals *ntIs1* V;*kyIs136* X were crossed with wild-type males of the CB4856 background (Hawaiian isolate), and recombinant progeny were isolated based on AWC and ASE axon guidance defects. In addition to the semidominance of the *chin-1*(*ns399*) mutation (see **Fig. 3** and relevant text), the *kpc-1;chin-1* double-mutants presented a partial maternal-rescue effect. Specifically, only 6 ± 1.2% of F2 progeny of double heterozygote F1s *kpc-1*(*0*/+)*;chin-1*(*ns399*/+) were defective in AIY axon NR entry. Yet 11.2 ± 0.8% F2s were expected to be defective, taking into account the Mendelian genetics and the penetrances of the double-mutants *kpc-1*(*gk8*)*;chin-1*(*ns399*), equal to 69.3% ± 6.1%, and those of the single mutants *kpc-1*(*gk8*) and *chin-1*(*ns399*) (17.5% ± 6.0% and 3.9% ± 2.3%, respectively). The difference between 6 ± 1.2% and 11.25 ± 1.25% (average ± s.e.m., $n = 4$ genotypes and 200 total animals) is statistically significant ($P = 0.02$). Since this partial maternal rescue effect affected the mutant penetrance of F2 homozygote mutant recombinants, animals of F2 progeny were clonally isolated blindly, and scoring of the relevant defects was performed only on the F3 progeny to isolate homozygous mutant recombinants. Linkage mapping and SNP analysis highlighted two positions linked to the mutant phenotype. One was refined to a ~3.1-cM interval of LG III – 25.76 cM (SNP K02F3.2: III:846,369) to III – 22.66 cM (SNP Y92C3A: III: 1,175,447). The second one was refined to a ~11.6-cM interval of LG III + 2.87 cM (SNP K02B12: I: 8,505,227) to III + 13.66 (SNP F15H9: I: 12,145,647). In the relevant LG I region, mutations were detected by WGS in 5 genes. The mutant was rescued with fosmid WRM0635bG07, which included *kpc-1*, and by a *kpc-1* cDNA under the ubiquitous promoter of the gene *dpy-30*. In the relevant LG III region, three mutations were detected by WGS. For two of those, fosmids were available, but when injected they gave no rescue. There was no fosmid available for the mutation present in the *chin-1* genomic locus. The *ns399* mutation was rescued using a *chin-1* cDNA under the ubiquitous promoter of the gene *dpy-30*. *Fmi-1* mutant alleles recovered in the enhancer screen of the *kpc-1*(*gk8*)*;mgIs18* background were tested for complementation with the reference allele *fmi-1*(*rh308*) and failed to complement. Mutants of interest were out-crossed at least four times.

CRISPR mutagenesis. CRISPR mutagenesis was performed as previously described[56]. N2 animals were injected with plasmid *dpy-10* sgRNA vector and with plasmid pGR255B containing the Cas9 and sgRNA target sequences for the genes *dpy-10* and *mab-20*. Repair oligo sequences were designed to reconstitute a *dpy-10*(*cn64*) allele, conferring a dominant Roller phenotype and resistant Dpy phenotype. F1s with *dpy-10* lesions resulting from active Cas9 were rollers and were cloned and tested for co-CRISPR in the *mab-20* locus. CRISPR changes in the targeted region of *mab-20* were detected using the Cel-1 enzyme[57] and the Surveyor Mutation Detection Kit. CRISPR resulted in generation of the allele *mab-20*(*ns789*), which contains a 3-bp insertion of ATA after 3024C, resulting in change of the motif VHSRVARV into VHSHSVARV and abolishing the Arginine247.

Furin motif prediction and deletion. Furins cleave target proteins at RXXR motifs; however, other cleavage sites are known[58]. We identified putative Furin cleavage sites in FMI-1 (Flamingo), MAB-20 (Semaphorin), and UNC-6 proteins by scanning for RXXR motifs and by using the predictions of an artificial neural network trained on known Furin cleavage sites (Prop1.0). We disrupted the motif by deleting the Arginine predicted to be recognized for cleavage and verified the disruption by accessing the Prop1.0 algorithm score of the deleted motif. In cases of adjacent Arginine motifs (RXXRXXR) the intermediate R was deleted to disrupt both of the neighboring motifs.

RNAi studies. RNAi was performed as previously described, using dsRNA-expressing vectors[59] or by feeding the worms dsRNA-expressing bacteria[60]. For RNAi by feeding, L3 animals were added to plates containing *E. coli* HT115 with pL4440 expression vectors targeting specific genes (Ahringer library, Vidal Library). Animals were grown at 20 °C for 4 d and progeny were scored.

Mosaic analysis. Mosaic analysis was performed as described previously[61,62]. *Kpc-1*(*gk8*)*;chin-1*(*ns399*) mutant animals were injected with unstable extrachromosomal transgene arrays, stochastically transmitted to daughter cells during cell divisions. We injected various arrays, consisting of a *kpc-1* rescuing fosmid WRM0635bG07 or *chin-1* under a ubiquitous promoter (*Pdpy-30::chin-1*, since there is no available fosmid bearing the *chin-1* locus) and markers of individual lineages as follows: *Pelt-2::mCherry* for intestine, *Pttx-3::mCherry* for the AIY neuron, *Pgly-18::myristoylated-GFP* for GLR cells, *Pmyo-2::GFP* for pharyngeal muscle, and *Pmir-228::myristoylated-GFP* for glia (this last allowed us to distinguish CEPsh glia from anterior labial glia and from amphid sheath glia). In this strategy, informative animals are very rare since they should keep the array overall but lose it only in specific tissues. Due to partial penetrance of the *kpc-1*(*gk8*)*;chin-1*(*ns399*) mutant, only animals with AIY defects were informative. Mutants in which the arrays segregate to intestinal or pharyngeal cells, to GLR mesodermal cells, or to AIY neurons, but not to CEPsh glia and SubL neurons, are not rescued

for AIY axon NR entry. Similarly, AIY axon defects are not rescued in mutants in which the unstable extrachromosomal arrays are present in anterior labial or amphid sheath glia but absent from the CEPsh glia (**Supplementary Table 2**). In studies of mosaic analysis, the presence of the array in the cells directly assayed does not preclude its presence in other cells not directly assayed.

Cell ablations. Cell ablation was performed by expressing cDNA of the pro-apoptotic EGL-1/BH3-only protein[63] under cell-type-specific promoters active prior to and during process outgrowth. Robust expression of the promoters used was detected in bean and later embryonic stages but not reported in the precursors of the cells of interest. EGL-1/BH3-only protein causes apoptosis when expressed ectopically[63]. Cell death was confirmed by absence of cell-specific marker expression in newly hatched larvae. For example, 24 of 120 EGL-1/BH3-only-expressing animals carrying the CEPsh-glia reporters *mir-228promoter::GFP* or *ptr-10promoter::RFP* lost fluorescent signal in 1–3 CEPsh glia (animals lacking all 4 were not observed, probably due to lethality). Animals also harboring a *ced-3*(*n717*) caspase mutation, preventing apoptosis, did not lose reporter expression (0 of 125).

Ablations of SubL neurons. Subsets of SubL neurons were ablated by expression of *Pceh-17:: egl-1* cDNA, expressed during bean and later stages in the SubL neurons SIAVL/R, SIADL/R, and SIBVL/R; the motor neurons DA5 and DA8; and in the noncommissural neurons ALA and RMED, starting after the comma stage. Cell ablation was detected postembryonically by absence of fluorescent reporters *Pceh-17::GFP/mCherry* labeling the four SubL neurons SIAVL/R and SIADL/R and the neuron ALA. SIBV neurons express *Pceh-17*-driven constructs as early and strongly as SIA neurons, and they are sisters to the SIAV neurons. Thus, SIBV cells most likely retain the provided transgene when SIAV neurons do and are likely killed along with the SIAV neurons. However, SIBV ablation was not directly assessed, due to the absence of SIBV-specific postembryonic reporters. In addition to SIA and SIBV neurons, these ablation experiments most likely killed the neurons DA5 and DA8, which are not part of the NR bundle, as well as the NR neurons ALA and RMED. ALA and RMED are located dorsally, further from the AIY and amphid-neuron axon growth, and their axon growth is not observed before 1.5-fold (G.R. and S.S., unpublished observations; Singhal *et al.*[64]), later than the SubL axons defining the NR. Moreover, *Pceh-17* is expressed in ALA/RMED only during or after the 1.5-fold stage, but not before, while by that time SIA/SIB axons have already formed the SubL, which defines the NR. Thus, while ALA/RMED were not directly assessed, these are less likely to have direct effects on early axon guidance of AIY and amphid neurons.

Ablations of CEPsh glia. Subsets of glia were ablated by expression of *Pmir-228::egl-1* cDNA. Cell ablation was detected by absence of CEPsh glia expression of fluorescent reporters *Pmir-228::GFP* (labeling all glia), *Pptr-10::RFP* (labeling all but amphid sheath glia (AMsh)), or *Phlh-17::myristoylated-GFP* (labeling CEPsh glia). In **Supplementary Table 1**, ablation of 'other glia' refers to the cases where CEPsh reporter expression was not abolished, but *Pmir-228::egl-1* was present in the animals (based on co-injection markers) and thus maybe present in other non-CEPsh glia. The large number (46), the close apposition, and the lack of specific reporters for all non-CEPsh glia precluded closely monitoring apoptosis of other glia. Highly penetrant axon-guidance defects were correlated with killing CEPsh glia. We cannot exclude effects of the OLQsh glia on axon guidance, since OLQshD are sisters of the CEPshD glia and thus likely obtain the *Pmir-228::egl-1* array when CEPsh glia do. However, during NR formation (bean–comma–1.5-fold embryos) the OLQshD are positioned in the tip of the nose (5–10 µm anterior to the NR axon growth)[14]. Moreover, none of their processes are reported to be included in the NR structure at any developmental stage during or after NR formation[65].

Axon defect scoring. Axon defects were detected by *Pceh-24::GFP* (labeling SubL neurons SIA, SIB, and SMD), *Pttx-3::mCherry* (labeling AIY neurons postembryonically), and *Podr-1::RFP* (labeling AWC/AWB amphid-commissure axons postembryonically). Misguided anterior processes were observed for SubL neurons, short axons were seen for AIY interneurons, and short axons or unfasciculated axon bundles were observed for AWC and AWB amphid commissure neurons. CEPsh morphology was scored using *Phlh-17::myristoylated-GFP*. Animals were scored after the end of embryogenesis. To correlate ablation with defects occurring in embryogenesis, we selected animals at the first larval stage (L1 larvae) containing the ablation constructs based on the presence of an embryonically expressed co-injection marker, and axon defects were scored without scoring cell ablation. Cell ablation was subsequently assessed. CEPsh ablation was specifically assessed in L3 larvae, where the glia reporters allow single-cell resolution of CEPsh glia from other anterior glia. Axon defects significantly correlated with CEPsh absence scored in later stages (AIY axon defects and SubL axon defects are significantly different in CEPsh ablated and non-CEPsh ablated animals, with $P = 0.0001$ for both comparisons; Fisher's test in GraphPad; **Supplementary Table 1**).

Imaging and defect scoring for postembryonic axons. Postdevelopmental live imaging and scoring of the AIY axon defects (by *mgIs18* or *otIs133*) was performed in L3–L4 animals (or L2 larvae when indicated). For scoring NR axon defects of neurons SIA, SIB, ASE, AFD, or PVQ, or CEPsh-glia membrane morphology, animals were anesthetized (with 20 mM sodium azide in M9 buffer), mounted on pads (2% agarose in H_2O), and examined on an Axioscope compound microscope (Zeiss). Twenty animals of L3–L4 larval stage (or L2 larvae when indicated) were mounted per slide and examined immediately after being anesthetized.

Quantification of axon defects. For population measurements of NR axon defects, animals were mounted on slides and visualized in an Axioscope compound microscope (Zeiss). Mutant phenotypes were quantified using axon markers to define NR entry and growth based on the meeting point of the dorsal-axon part of bilaterally symmetrical neurons. When scoring axons of ASE or AIY neurons, wild-type animals show a full axonal ring with a dorsal meeting point of bilaterally symmetrical axons, while mutant animals present an axonal ring with a gap and no dorsal meeting point. Images presented in **Figure 3a–h** are of L3–L4 animals, for better visualization of the defect. Scoring of mutant phenotypes was performed in animals of early larval stages L1–L3. No significant difference of defects was observed in between L1 and L4 larval stages, i.e., AIY axons were defective in 17 of 20 L1 animals and in 14 of 19 L4 animals (nonsignificant difference assessed by Fisher's test (in GraphPad), $P = 0.8130$).

For embryonic axon-length measurements, images were acquired on a Deltavision microscope, as described below. Axons were traced and axon length was measured manually using image stacks in ImageJ/Fiji. Axon length was measured from the anterior limit of cell body fluorescence to the anterior limit of axon fluorescent tip.

Deltavision microscopy imaging of embryonic samples. Embryos at late ball stage were mounted on a 5% agar pad without azide and were washed repeatedly to remove bacteria before mounting. Images were collected using a Weatherstation environmental chamber set at 20 °C on a DeltaVision Image Restoration Microscope (Applied Precision) with an Inverted Olympus IX-70 microscope and using a 63× silicone oil-immersion objective and a Photometrics CoolSnap HQ camera (Roper Scientific). Time-lapse images were acquired until the embryo began to twitch at early 1.5-fold stage. A stack of optical sections at 0.5-µm spacing was acquired at 12-min intervals, using conditions for non-saturated signal, 10–32% power, and exposure times of 0.2–0.5 s, depending on the labeling reporter used. Image acquisition did not result in appreciable developmental arrest. Between timepoints the focal midpoint of the stack was adjusted to compensate for rotation of the embryo and movement of the cell of interest. Deconvolution of DeltaVision Images was performed with Softworx (Applied Precision).

Quantification of FMI-1-GFP localization defect. The same integrated transgene of FMI-1-GFP (under *fmi-1* endogenous regulatory sequences) was crossed into genetic backgrounds of *chin-1*(*ns399*);*kpc-1*(*gk8*) double-mutants, or single mutants *chin-1*(*ns399*) and *kpc-1*(*gk8*). *chin-1* single mutants occasionally exhibit embryo-wide FMI-1-GFP misexpression. This misexpression is likely irrelevant to the NR defects, as it is not observed in *kpc-1;chin-1* double-mutants and may result from background mutation(s). Embryos presenting this embryo-wide misexpression were excluded from the imaging analysis to avoid differences in signal localization that are irrelevant to our genes and phenotypes of interest.

Embryo samples expressing integrated FMI-1-GFP (under *fmi-1* endogenous regulatory sequences) were collected in M9 buffer and mounted on pads (2% agarose in H2O). Images were acquired in Inverted TCS SP8 laser scanning confocal microscope (Leica), using the same scanning microscope (with same objective, HyD hybrid detector) and the same acquisition parameters (laser wavelength,

doi:10.1038/nn.4630

zoom magnification, exposure time, *z*-step size, field size, pinhole = 1, etc.) between wild-type and mutant samples. Embryos of different genotypes were synchronized at the 1.5-fold stage. Samples were quantitatively analyzed only when comparable based on the following criterion: measurement of the length of the 'elongation fold' between the tail and the tail fold-depression should be 16–18 µm. Embryos with smaller or larger length values were excluded, to control sample variability. Sum projections were acquired from whole embryo stacks, region of interest (ROI) were selected, and intensities of ROI were quantified using ImageJ (NIH, USA). ROI sizes (**Fig. 5**) were of the following sizes: region I (neuropil cell bodies: 7 µm high, 20 µm wide), region II (NR bundle: 7 µm high, 20 µm wide), region III (sensory dendritic endings: 6 µm high, 15 µm wide), and region IV (background in the dorsal part of the tail fold: 7 µm high, 20 µm wide). In each sum projection, the mean intensity of background (region IV) was subtracted from the mean or maximum intensities of the ROI (I, II, and III). Comparisons were made between mean or maximum intensities of ROI-I and ROI-II or ROI-I and the sum of ROIs I, II, and III. A *t* test was used for statistical analysis. The background intensity values of ROI-IV between samples of different genotypes was not significantly different, i.e., the background intensity values of WT compared to *kpc-1;chin-1* double-mutant animals represented in **Figure 6e** were not significant; two-tailed $P = 0.179$, $t = 1.3660$; *t* test in GraphPad).

Image processing. Maximum or sum projections were prepared using ImageJ/Fiji. Top views (top from head) of the NR were rendered by the 'Stack Reslice' parameter in ImageJ/Fiji. Image projections used for qualitative analysis were adjusted for brightness, contrast, and false color indexing using Photoshop CS4 (Adobe Software). When reporters labeled neurons of different identities (*Pttx-3* labeling AIY and SMDD, *Phlh-16* labeling both SMDD and AWC), pseudocoloring for purposes of representation was performed as follows: cells were identified based on expression pattern, cell positioning, and process morphology as previously defined[14,54], and maximum projections corresponding to each of the two neurons labeled were acquired and color-coded using ImageJ. Merged color images were assembled using the layer mode in Photoshop. Movies were assembled using QuickTime Pro and Final Cut Pro.

Embryo/L1 sample preparation for stage synchronization. Adults were cut open and embryos were selected and synchronized at the two-cell or four-cell stage. These embryos were grown at 20 °C and selected after 310–320 min (for two-cell stage embryos) or 290–310 min (for four-cell stage embryos) for late ball stage embryos (**Fig. 4g**) and 20 min, 40 min, or 60 min later for bean stage, comma stage, and 1.5-fold stage embryos, respectively. For L1 animals, embryos were selected and synchronized by morphology at the 1.5-fold stage. L1 animals were picked after growing at 20 °C for 400–450 min.

Electron microscopy sample preparation and imaging. Embryos were synchronized as described above. Samples were prepared for electron microscopy using standard methods[66]. Ultrathin serial sections (70 nm) were collected using a Leica Ultracut UCT Ultramicrotome. Sections at head regions were examined. Electron microscopy images were acquired using a FEI Tecnai G2 Spirit BioTwin transmission electron microscope operating at 120 kV with a Gatan 4K × 4K digital camera.

FIB-SEM microscopy. Focused ion beam scanning electron microscope (FIB-SEM) was performed at the NY Structural Biology Center using a Dual beam FEI Helios NanoLab 650 instrument. A modified high-contrast *en bloc* staining OTO method[67] was applied to the FIB-SEM specimen preparation. Sodium thiocarbohydrazide (TCH) was used to bind the primary osmium stain. Then, the *en bloc* stain was enhanced by a second round of osmium fixation. Glutaraldehyde (1%) was added to provide effective protein crosslinking in tissues. The fixed samples were embedded in Eponate 12 resin (TedPella). The serial sections before the ROI were searched and confirmed by TEM imaging before the critical portion of the specimen was reached. Sample blocks were mounted on scanning electron microscope (SEM) stubs using double-sided carbon sticky tape, then painted with colloidal silver (EMS). The sample blocks were made conductive by coating them with palladium in a Denton sputter coater (25 mA current for 5 min at 50–60 mTorr) then inserted into the FEI Helios NanoLab 650 (FEI) vacuum chamber. Areas were identified by viewing with the e-beam at 20 keV, then coated with 1-µm-thick platinum for specimen surface protection. We collected serial images with FEI AutoSlice and View software, using a slice width of 30 nm and a horizontal field width of 18.7 µm. Sections were imaged at an e-beam voltage of 2 keV and 100 pA current. The focus and stigmation of the electron beam was continuously checked and optimized by the AutoSlice and View as the FIB continued to mill into a sample and the imaging face receded. Following collection, accurate image registration was achieved by applying a scale-invariant features algorithm[68] to the raw image stacks. The image *x–y* resolution of the acquired FIB-SEM images is 4.56 nm/pixel. L1 animals of N2 (wild-type) or *chin-1*(*ns399*);*kpc-1*(*gk8*) strains were used for the FIB-SEM, synchronized as described above.

Sample preparation for heat-shock studies. Synchronization was performed as described above. Transgenic embryos expressing rescuing constructs were distinguished from the non-transgenics before morphogenesis, by the extrachromosomal expression of RFP under a ubiquitous promoter driving early embryonic expression (*Pubq-1*). These embryos were grown at 20 °C and relevant embryonic stages were heat-shocked at 30 °C in an incubator for 5 min, then allowed to recover for 34 h at 20 °C. Two days later, hatched animals were scored as L3s for NR defects of the AIY axon.

Dye filling assays. Animals were washed off NGM plates with M9 medium and spun down briefly in a microcentrifuge. The supernatant was removed, and the lipophilic dye 1,1′-dioctadecyl-3,3,3′,3′-tetramethylindocarbocyanine perchlorate (DiI, prepared in N,N-dimethylformamide) was added at 10 µg/mL in M9. Animals were then soaked in dye for 60 min in the dark, washed twice with M9, and mounted on slides to be scored for amphid-commissure axon defects in Axioscope compound microscope (Zeiss). Amphid commissures presented variable defects: thinner bundles, indicating at least some amphid axons prematurely stopped; or aberrant processes, primarily guided to the anterior of the NR bundle, likely following aberrant SubL neurons.

Yeast-two-hybrid screen. Yeast-two-hybrid screening was performed using the Dual Y2H kit (DUALSYSTEMS Biotech). N-terminal fusions of LexA and Gal4 domains were used. Candidate interactions were tested between dominant GAD-CHIN-1(R270A) and DBD-GTPase fusions of dominant Q61L mutant variants that stabilized GAP–GTPase binding[69]. The following RhoGTPases were assayed: CED-10, RAB-2, RAB-6.1, RAB-6.2, RAB-7, RAB-11, and CDC-42. Plates with or without Histidine (His^+ or His^-) were used, respectively, for growth or to detect interactions.

Statistics. The sample sizes and statistical tests were chosen based on previous studies with similar methodologies; the data met the assumptions for each statistical test performed. No statistical method was used to decide sample sizes. All experiments were performed three or four times, as indicated, yielding similar results and comprised of biological replicates. Independent transgenic lines or individual days of scoring for mutant strains were treated as independent experiments for calculating the s.e.m. Fisher's test (GraphPad) was used to measure the statistical significance of AIY or SubL axon NR defects. For comparison of normally distributed values of intensities of FMI-1-GFP, we used student's *t* test (GraphPad). For all figures, the mean ± s.d. is represented, unless otherwise noted. *P* values were calculated using GraphPad software, and we used Prism to calculate the difference between each set of pairs, keeping track of sign. The *t* ratio for a paired *t* test presents the mean of these differences divided by the standard error of the differences. The number of degrees of freedom equals the number of pairs minus 1.

Blinding and randomization during data analysis. Blinding during data analysis was not performed, with the following exceptions. In cell-ablation experiments (**Fig. 2e–h**), axon defects were quantified before determining the presence or absence of CEPsh glia. During electron microscopy experiments on L1 animals (FIB-SEM; **Fig. 2i–l**), the genotype of L1 animals analyzed was unknown to the researcher performing EM preparation and imaging. During yeast-two-hybrid screening experiments (**Fig. 6h**), analysis of Y2H interactions of CHIN-1 with candidate GTPases was performed blindly; the genetic identity of the clones analyzed was unknown to the researcher quantifying strength of interactions. Samples were allocated to groups of the genetic background (genotype), detected by standard genetic/genomic approaches. Otherwise, samples were randomly selected within these groups, based on previous studies with similar methodologies.

Life sciences reporting summary. A summary of experimental design and software used is also provided in the **Life Sciences Reporting Summary**.

Availability of data. The datasets generated and/or analyzed during the current study are either included in this published article (and its Supplementary Information files) or available from the corresponding author on reasonable request.

51. Brenner, S. The genetics of *Caenorhabditis elegans*. *Genetics* **77**, 71–94 (1974).
52. Stiernagle, T. Maintenance of *C. elegans*. In *C. elegans* (ed. Hope, I.A.) 51–67 (Oxford, 1999).
53. Mello, C.C., Kramer, J.M., Stinchcomb, D. & Ambros, V. Efficient gene transfer in *C.elegans*: extrachromosomal maintenance and integration of transforming sequences. *EMBO J.* **10**, 3959–3970 (1991).
54. Sulston, J.E. & Horvitz, H.R. Post-embryonic cell lineages of the nematode, *Caenorhabditis elegans*. *Dev. Biol.* **56**, 110–156 (1977).
55. Hedgecock, E.M., Culotti, J.G., Thomson, J.N. & Perkins, L.A. Axonal guidance mutants of *Caenorhabditis elegans* identified by filling sensory neurons with fluorescein dyes. *Dev. Biol.* **111**, 158–170 (1985).
56. Dickinson, D.J., Ward, J.D., Reiner, D.J. & Goldstein, B. Engineering the *Caenorhabditis elegans* genome using Cas9-triggered homologous recombination. *Nat. Methods* **10**, 1028–1034 (2013).
57. Ward, J.D. Rapid and precise engineering of the *Caenorhabditis elegans* genome with lethal mutation co-conversion and inactivation of NHEJ repair. *Genetics* **199**, 363–377 (2015).
58. Duckert, P., Brunak, S. & Blom, N. Prediction of proprotein convertase cleavage sites. *Protein Eng. Des. Sel.* **17**, 107–112 (2004).
59. Tavernarakis, N., Wang, S.L., Dorovkov, M., Ryazanov, A. & Driscoll, M. Heritable and inducible genetic interference by double-stranded RNA encoded by transgenes. *Nat. Genet.* **24**, 180–183 (2000).
60. Kamath, R.S. *et al.* Systematic functional analysis of the *Caenorhabditis elegans* genome using RNAi. *Nature* **421**, 231–237 (2003).
61. Heiman, M.G. & Shaham, S. DEX-1 and DYF-7 establish sensory dendrite length by anchoring dendritic tips during cell migration. *Cell* **137**, 344–355 (2009).
62. Yochem, J. & Herman, R.K. Investigating *C. elegans* development through mosaic analysis. *Development* **130**, 4761–4768 (2003).
63. Conradt, B. & Horvitz, H.R. The *C. elegans* protein EGL-1 is required for programmed cell death and interacts with the Bcl-2-like protein CED-9. *Cell* **93**, 519–529 (1998).
64. Singhal, A. & Shaham, S. Infrared laser-induced gene expression for tracking development and function of single C. elegans embryonic neurons. *Nat Commun* **8**, 1–13 (2017).
65. Ward, S., Thomson, N., White, J.G. & Brenner, S. Electron microscopical reconstruction of the anterior sensory anatomy of the nematode *Caenorhabditis elegans*. *J. Comp. Neurol.* **160**, 313–337 (1975).
66. Bargmann, C.I., Hartwieg, E. & Horvitz, H.R. Odorant-selective genes and neurons mediate olfaction in *C. elegans*. *Cell* **74**, 515–527 (1993).
67. Seligman, A.M., Wasserkrug, H.L. & Hanker, J.S. A new staining method (OTO) for enhancing contrast of lipid--containing membranes and droplets in osmium tetroxide--fixed tissue with osmiophilic thiocarbohydrazide(TCH). *J. Cell Biol.* **30**, 424–432 (1966).
68. Lowe, D.G. Object recognition from local scale-invariant features. *Proc. Seventh IEEE Int. Conf. Comput. Vis.* **2**, 1150–1157 (1999).
69. Scheffzek, K. *et al.* The Ras-RasGAP complex: structural basis for GTPase activation and its loss in oncogenic *Ras* mutants. *Science* **277**, 333–338 (1997).

doi:10.1038/nn.4630

nature research

Corresponding author(s): Georgia Rapti
Shai Shaham

☐ Initial submission ☐ Revised version ☒ Final submission

Life Sciences Reporting Summary

Nature Research wishes to improve the reproducibility of the work that we publish. This form is intended for publication with all accepted life science papers and provides structure for consistency and transparency in reporting. Every life science submission will use this form; some list items might not apply to an individual manuscript, but all fields must be completed for clarity.

For further information on the points included in this form, see Reporting Life Sciences Research. For further information on Nature Research policies, including our data availability policy, see Authors & Referees and the Editorial Policy Checklist.

Experimental design

1. Sample size

Describe how sample size was determined.

The sample size and statistical tests were chosen based on previous studies with similar methodologies and the data met the assumptions for each statistical test performed. No statistical method was used in deciding sample sizes.

2. Data exclusions

Describe any data exclusions.

Images were excluded from quantification when fluorescence irrelevant to the genetic background studied was observed, as described in the Supplemental Material and Methods Section.

3. Replication

Describe whether the experimental findings were reliably reproduced.

All experiments were performed 3 or 4 times, as indicated, yielding similar results and comprised of biological replicates. Independent transgenic lines or individual days of scoring for mutant strains were treated as independent experiments for standard error of the mean.

4. Randomization

Describe how samples/organisms/participants were allocated into experimental groups.

Samples were allocated to groups of the genetic background (genotype), detected by standard genetic/ genomic approaches. Otherwise samples were randomly selected within these groups, based on previous studies with similar methodologies.

5. Blinding

Describe whether the investigators were blinded to group allocation during data collection and/or analysis.

Investigators performed phenotypic analysis without taking into account the genotype of sample groups, when possible.

Note: all studies involving animals and/or human research participants must disclose whether blinding and randomization were used.

Nature Neuroscience: doi:10.1038/nn.4630

6. Statistical parameters

For all figures and tables that use statistical methods, confirm that the following items are present in relevant figure legends (or in the Methods section if additional space is needed).

n/a	Confirmed
☐	☒ The exact sample size (*n*) for each experimental group/condition, given as a discrete number and unit of measurement (animals, litters, cultures, etc.)
☐	☒ A description of how samples were collected, noting whether measurements were taken from distinct samples or whether the same sample was measured repeatedly
☐	☒ A statement indicating how many times each experiment was replicated
☐	☒ The statistical test(s) used and whether they are one- or two-sided (note: only common tests should be described solely by name; more complex techniques should be described in the Methods section)
☐	☒ A description of any assumptions or corrections, such as an adjustment for multiple comparisons
☐	☒ The test results (e.g. *P* values) given as exact values whenever possible and with confidence intervals noted
☐	☒ A clear description of statistics including central tendency (e.g. median, mean) and variation (e.g. standard deviation, interquartile range)
☐	☒ Clearly defined error bars

See the web collection on statistics for biologists for further resources and guidance.

Software

Policy information about availability of computer code

7. Software

Describe the software used to analyze the data in this study.	Microscopy images were prepared using ImageJ/Fiji and in some cases were adjusted using Photoshop CS4 (Adobe Software). Electron microscopy images were acquired using FEI AutoSlice and View™ software. Movies were assembled using QuickTime Pro and Final cut Pro.

For manuscripts utilizing custom algorithms or software that are central to the paper but not yet described in the published literature, software must be made available to editors and reviewers upon request. We strongly encourage code deposition in a community repository (e.g. GitHub). *Nature Methods* guidance for providing algorithms and software for publication provides further information on this topic.

Materials and reagents

Policy information about availability of materials

8. Materials availability

Indicate whether there are restrictions on availability of unique materials or if these materials are only available for distribution by a for-profit company.	All unique materials used are available from standard commercial sources or will be available from the authors upon reasonable request.

9. Antibodies

Describe the antibodies used and how they were validated for use in the system under study (i.e. assay and species).	No antibodies were used in this study.

10. Eukaryotic cell lines

a. State the source of each eukaryotic cell line used.	No eukaryotic cell lines were used in this study.
b. Describe the method of cell line authentication used.	No eukaryotic cell lines were used in this study.
c. Report whether the cell lines were tested for mycoplasma contamination.	No eukaryotic cell lines were used in this study.
d. If any of the cell lines used are listed in the database of commonly misidentified cell lines maintained by ICLAC, provide a scientific rationale for their use.	No eukaryotic cell lines were used in this study.

Nature Neuroscience: doi:10.1038/nn.4630

Animals and human research participants

Policy information about studies involving animals; when reporting animal research, follow the ARRIVE guidelines

11. Description of research animals

Provide details on animals and/or animal-derived materials used in the study.	Nematodes of the species Caenorhabditis elegans were used in this study.

Policy information about studies involving human research participants

12. Description of human research participants

Describe the covariate-relevant population characteristics of the human research participants.	No human researcher participants were used in this study.

Nature Neuroscience: doi:10.1038/nn.4630